PREPARATION OF Pd-Pt/AL_2O_3 BIMETALLIC CATALYST WITH CHARGE ENHANCED DRY IMPREGNATION METHOD

NEOH KUANG HONG

A project report submitted in partial fulfilment of the requirements for the award of Bachelor of Engineering (Hons.) Chemical Engineering

Faculty of Engineering and Science
Universiti Tunku Abdul Rahman

April 2015

DECLARATION

I hereby declare that this project report is based on my original work except for citations and quotations which have been duly acknowledged. I also declare that it has not been previously and concurrently submitted for any other degree or award at UTAR or other institutions.

Signature : _____

Name : _____

ID No. : _____

Date : _____

APPROVAL FOR SUBMISSION

I certify that this project report entitled **"PREPARATION OF Pd-Pt/AL_2O_3 BIMETALLIC CATALYST WITH CHARGE ENHANCED DRY IMPREGNATION METHOD"** was prepared by **NEOH KUANG HONG** has met the required standard for submission in partial fulfilment of the requirements for the award of Bachelor of Engineering (Hons.) Chemical Engineering at Universiti Tunku Abdul Rahman.

Approved by,

Signature : _____

Supervisor : _____

Date : _____

Specially dedicated to
my beloved grandmother, mother and father

ACKNOWLEDGEMENTS

I would like to thank everyone who had contributed to the successful completion of this project. I would like to express my gratitude to my research supervisor, Dr. Yap Yeow Hong for his invaluable advice, guidance and his enormous patience throughout the development of the research.

In addition, I would also like to express my gratitude to my loving parent and friends who had helped and given me encouragement.

Furthermore, I would like to thank Mr. Ooh Keng Fai in UTAR Perak Campus for his time and effort in running the field emission scanning electron microscopy (FESEM) analysis.

Last but not least, I wish to extend to gratitude to Tai Xiao Hwa and Ng Yee Fhan who have been the best companions throughout the research.

PREPARATION OF Pd-Pt/Al_2O_3 BIMETALLIC CATALYST WITH CHARGE ENHANCED DRY IMPREGNATION METHOD

ABSTRACT

Often, metal supported catalysts prepared by dry impregnation suffer from absence of metal precursor-support interactions which leads to poor metal dispersion. Additionally, catalysts prepared from single metal also tend to suffer from premature deactivation due to sintering compared to bimetallic catalysts. Ongoing research on bimetallic catalysts has shown that the addition of second metal improves stability and activity of the catalysts. In the light of this, Pd-Pt bimetallic catalyst supported on γ-alumina were prepared using charge enhanced dry impregnation (CEDI) method. CEDI method has the capability to induce strong metal precursor-support interaction and therefore improve the metal dispersion. In this project, chloroplatinic acid (CPA) and palladium (II) chloride ($PdCl_2$) were used as the metal precursors to prepare the bimetallic catalyst. Two sets of catalysts samples were prepared. The first set studied the effect of atomic ratio of Pt:Pd on the reducibility of catalyst while the second set studied the effect of impregnation method (coimpregnation and sequential impregnation) on the metallic structure (alloy or core-shell) of prepared catalysts. All samples were characterised by X-ray diffraction (XRD), temperature programmed reduction (TPR), scanning electron microscopy (SEM) and energy-dispersive X-ray spectroscopy (EDXS). The results from EDXS reveal that CEDI were able to produce Pd-Pt/Al_2O_3 bimetallic catalyst with high dispersion. According to TPR results, Pd-Pt/Al_2O_3 bimetallic catalyst with a higher atomic ratio of Pt:Pd has lower reducibility. The same situation was observed in the case of sequential impregnated Pd-Pt/Al_2O_3. Furthermore, results from TPR also suggest that coimpregnated Pd-Pt/Al_2O_3 contains alloy of Pd-Pt while sequential impregnated Pd-Pt/Al_2O_3 is of core-shell structure.

TABLE OF CONTENTS

LIST OF TABLES

LIST OF FIGURES

LIST OF SYMBOLS / ABBREVIATIONS

A	specific surface area of oxide, m^2/g
A_s	nitrogen cross sectional area, m^2
C	metal precursor concentration, mol/L
C_e	solution concentration at equilibrium, mol/L
C_{final}	final concentration of impregnating solution, µg/L
$C_{initial}$	initial concentration of impregnating solution, µg/L
k^+	adsorption rate constant, L/(mol·s)
k^-	desorption rate constant, s^{-1}
K	BET constant
K	equilibrium adsorption constant
m	mass of oxide, g
M	molecular weight, g/mol
MW	molecular weight of metal, µg/µmol
n	surface concentration, µmol/g
n_s	saturation capacity, µmol/g
N	Avogadro's constant, mol^{-1}
P/P_0	relative pressure
P_a	Ambient pressure, atm
R	Gas constant, L·atm/(K·mol)
S	specific surface area, m^2/g
t	time, s
T	Ambient temperature, K
V	volume of impregnating solution, L
V_{ads}	Volume of gaseous nitrogen adsorbed, L
V_m	Molar volume of liquid nitrogen, L/mol
V_p	total pore volume, L
w	weight of sample catalyst, g

W	weight of nitrogen adsorbed, g
W_m	weight of nitrogen as monolayer, g
λ	wavelength, Å
Γ	adsorption density, nmol/m^2
BET	Brunauer-Emmett-Teller
CEDI	charge enhanced dry impregnation
CPA	chloroplatinic acid
DI	dry impregnation
EDXS	energy-dispersive X-ray spectroscopy
FESEM	field emission scanning electron microscopy
ICP-OES	inductively-coupled plasma optical emission spectroscopy
PTA	platinum tetramine
PZC	point of zero charge
RDP	reduction deposition precipitation
TCD	thermal conductivity detector
TEM	transmission electron microscopy
TPD	temperature programmed desorption
TPR	temperature programmed reduction
SEA	strong electrostatic adsorption
SEM	scanning electron microscopy
SL	surface loading, m^2/L
WI	wet impregnation
XRD	X-ray diffraction

LIST OF APPENDICES

CHAPTER 1

INTRODUCTION

1.1 Background

Catalysis is the use of a catalyst to increase the rate of reaction. A catalyst is a substance that is not consumed or changed at the end of the reaction. Its function is to lower down the activation energy required to initiate a chemical reaction. As a result, the reaction rate of a catalysed reaction is higher than that of an uncatalysed reaction at the same temperature. At the same time, a catalyst improves selectivity, that is, the ratio of rate of reaction of desired reaction to rate of reaction of undesired reaction.

In general, there are two types of catalysts, namely homogeneous catalyst and heterogeneous catalyst. A homogeneous catalyst is a catalyst that exists in the same phase as the reactants whereas a heterogeneous catalyst is a catalyst that is in a different phase than the reactants. A heterogeneous catalyst is often available in solid state and used to catalyse liquid or gaseous reactants. Emphasis will be given to heterogeneous catalyst in this report.

Catalysts play an indispensible role in chemical industry, electricity generation, food processing and environmental pollution control.

In chemical industry, catalysts are used extensively to increase production rate and decrease energy consumption. Perhaps one of the most well-known catalytic chemical processes is the Haber process which synthesises ammonia from nitrogen and hydrogen. Prior to the invention of Haber process, ammonia was mainly

produced by dry distillation of mineral coal which had limited reserve (Ekstrand, 1966). In Haber process, ammonia is synthesised reversibly from nitrogen and hydrogen under pressure (200 atm) and elevated temperature (400 ^{o}C). The chemical equation is given below:

$$N_2 + 3H_2 \Leftrightarrow 2NH_3 \qquad (1.1)$$

Promoted iron catalyst is employed to favour the forward reaction. Without the presence of catalyst, synthesis of ammonia will be difficult. To provide a bigger perspective, the main applications of other important catalysts in chemical industry are shown in Table 1.1.

Table 1.1: Catalysts with Their Main Applications (Ross, 2012)

Catalyst	Applications
Ni/Al_2O_3	Fat hardening
Ag/Al_2O_3	Ethylene oxidation
Pt/Rh gauze	Ammonia oxidation
$Cu/ZnO/Al_2O_3$	Methanol synthesis
Co/SiO_2	Fischer-Tropsch synthesis
Ni/Al_2O_3	Steam methane reforming

One way of generating electricity is through catalytically combusting methane in gas turbine combustors (Persson, 2006). Methane is combusted over catalysts wherein the combustion temperature can be decreased with improved oxidation of methane. This in turn leads to low level emission of pollutants like nitrogen oxides, carbon monoxide and unburned hydrocarbons.

One of the uses of catalysts in food processing industry is the hydrogenation of unsaturated fatty acids to saturated fatty acids of edible oils (Shafii *et al.*, 2012). When fatty acids undergo hydrogenation process, not all carbon double bonds are saturated. Those unhydrogenated fatty acids tend to isomerise from cis to trans fatty

acids (Stanković *et al.*, 2009) which are bad for health when consumed (Singh, Rezac and Pfromm, 2010). Catalysts have been shown to facilitate the hydrogenation of fatty acids and thus hinder the formation of trans fatty acids (Shafii *et al.*, 2012).

Besides, catalysts are also applied for environmental pollution control. One prominent example is the use of catalytic converters in automobiles exhaust. Platinum and palladium deposited in the monoliths of catalytic converters convert toxic gases such as oxides of nitrogen, carbon monoxide and unburned hydrocarbons to non-lethal nitrogen, carbon dioxide and water. Recently, Hussain *et al.*, (2009) developed a titanium dioxide supported Ru-Mn-Co trimetallic catalyst which converts carbgas (CO_2 + H_2O + H_2) as a measure to control the emission of carbon dioxide which is a greenhouse gas.

Nevertheless, the conventional catalysts in use are typically monometallic catalysts. Monometallic catalysts are catalysts with only one type of active metal. In catalytic combustion of methane, Narui *et al.*(1999) has shown that monometallic Pd catalyst has poor stability as time progresses. Persson, Jansson and Järås (2007) also produced the same result. They showed that the activity of fresh Pd catalysts was high but plummeted severely in the course of the combustion operation. Poor stability leads to diminished activity of the catalyst.

Many studies have been done to find a way to stabilise or to outperform monometallic catalysts. One of the ways is to include an extra metal to form a bimetallic catalyst. One such metal is platinum (Narui *et al.*, 1999). Persson, Jansson and Järås (2007) have shown that the activity of bimetallic Pd-Pt catalysts increases slightly when compared to that of monometallic Pd catalysts which decreases significantly in prolonged reaction time. Apart from that, use of bimetallic catalysts can also lead to higher selectivity. For example, Li *et al.* (2008) showed that the amount of trans fatty acids remained in soybean oil after undergoing hydrogenation by Ni-B bimetallic catalyst were around half the amount of trans fatty acids produced using monometallic Ni catalyst.

Indeed, the superiority of bimetallic catalysts over monometallic catalysts in increasing activity, conversion and yield of a certain reaction has gained much attention from the chemical industry (Yu, Porosoff and Chen, 2012).

1.2 Problem Statement

Solid catalysts are normally made up of precious metals. Examples of precious metals are nickel, palladium, platinum, rhodium and etc. Since these precious metals used for synthesis of catalyst are rare and expensive, there is a need to effectively utilise these metals to obtain the best performance. Traditionally, metal nanoparticles are dispersed onto metal oxide support such as alumina to achieve high activity. But still, some catalysts have limitations such as short lifetime due to premature deactivation of the catalysts.

1.3 Aims and Objectives

The aim of this final year project is to explore and prepare bimetallic Pd-Pt/Al_2O_3 catalysts with high dispersion of metal nanoparticles. There are a few sub-objectives:

1. To determine the effect of atomic ratio of platinum to palladium on the characteristics of catalyst.
2. To investigate the effect of impregnation method (coimpregnation or sequential impregnation) on the characteristics of catalyst.

1.4 Scope

A range of Pd-Pt/Al_2O_3 catalyst with different Pt:Pd ratio was prepared using charge-enhanced dry impregnation (CEDI) method. In addition, coimpregnated and sequential impregnated Pd-Pt/Al_2O_3 catalysts were also prepared using CEDI method. Several catalyst characterisation tests were then carried out. They were:

- Determination of point of zero charge (PZC) of γ-alumina
- Determination of pH for optimal adsorption of metal particles
- X-ray Diffraction (XRD)
- Temperature programmed reduction (TPR)
- Scanning electron microscopy (SEM)
- Energy-dispersive X-ray spectroscopy (EDXS)

CHAPTER 2

LITERATURE REVIEW

2.1 Types of Catalyst

2.1.1 Homogeneous versus Heterogeneous

In general, catalysts can be categorised into two groups, namely homogeneous catalysts and heterogeneous catalyst. A homogeneous catalyst is a catalyst with the same phase as the reactants. Homogeneous catalysts can range from organometallic complexes, enzymes, Lewis acids to metal ions (Farnetti, Di Monte and Kašpar, *n.d.*). Examples of homogeneous catalysis are rhodium-catalysed carbonylation of methanol and CO to form acetic acid, cobalt-catalysed hydroformylation of propylene, CO and hydrogen to form n-butyraldehyde and molybdenum-catalysed epoxidation of propylene to form propylene oxide (Bhaduri and Mukesh, 2000). It should be noted that the metals stated above exist in the form of organometallic complexes which is soluble in reaction medium. Metals in their solid form are used in heterogeneous catalysis instead.

A heterogeneous catalyst is a catalyst with distinct phase from the reactants. The most common heterogeneous catalysts are metal catalysts which comprise of precious and rare metals such as platinum, palladium, nickel, rhodium, ruthenium and etc. They are available in both unsupported and supported forms.

Unsupported metal catalysts take many forms: single catalysts, powders, wires, ribbons and many more. Active sites are found on the surface of the metals.

They are effective sites that are responsible for a particular catalytic reaction (Haber, 1991). The active sites of unsupported catalysts are highly exposed to the reaction medium because these catalyst particles are very fine and thus comprise of high specific surface area. Although higher specific surface area is able to increase the rate of reaction, tiny particles in the form of powder are prone to sintering. Sintering is the agglomeration of these particles into a large particle when subjected to high temperature. This results in a drop of specific surface area, making unsupported catalysts less efficient (Augustine, 1995). Furthermore, separation of catalyst from the product can become an issue.

Therefore, supported catalysts were invented to prevent sintering of metal particles and facilitate better separation between products and catalysts. The support usually possesses high porosity, which creates high specific surface area for which the particles are anchored to. In this case, sintering can be avoided or at least minimised in supported catalysts as the metal crystallites are widely scattered. As a comparison, Augustine (1996) stated that the sintering temperature of a powdered platinum catalyst (unsupported catalyst) was around 350–400 ^{o}C lower than that of a catalyst with platinum on alumina support. This means that the powdered platinum catalyst was more susceptible to sintering.

In heterogeneous catalytic reaction for supported catalysts, it is essential to study the diffusion of reactants inside the support in order to determine the rate limiting step. Figure 2.1 shows the pathway of diffusion of reactant A to and from the pores of the catalyst support to give product B. Descriptions are presented below the figure.

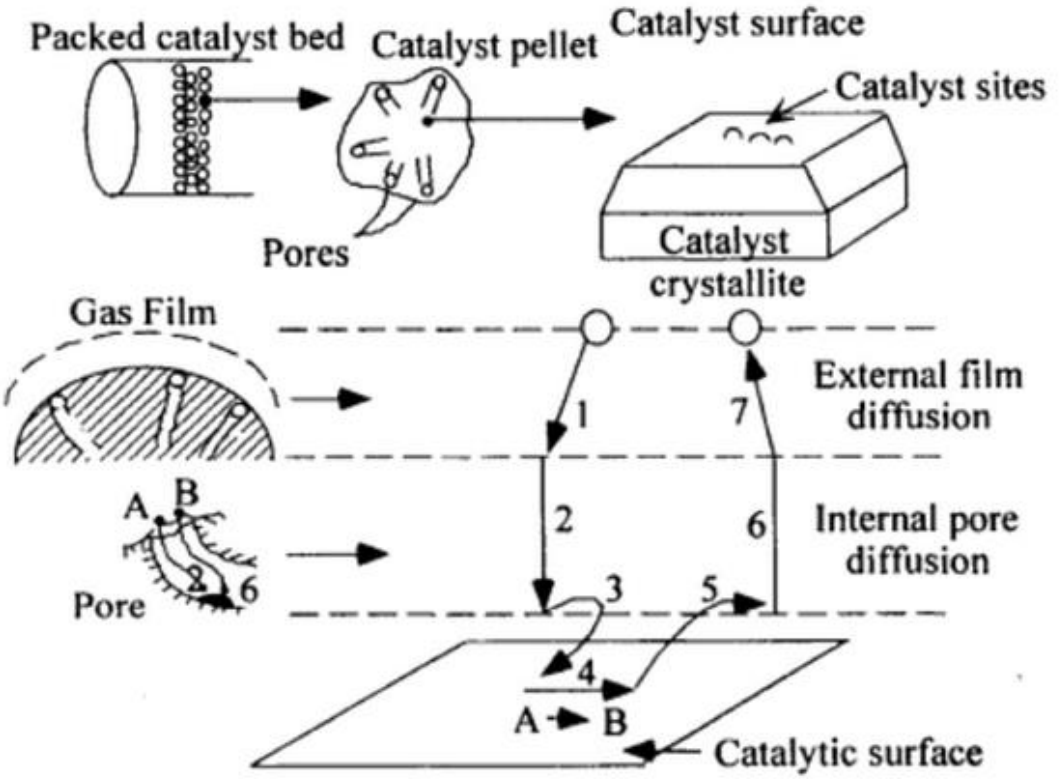

Figure 2.1: Steps in a Heterogeneous Catalytic Reaction in a Porous, Supported Catalyst (Fogler, 2006)

1) Bulk diffusion of A through the boundary later surrounding the catalyst support to the external catalyst surface.
2) Diffusion of A by either bulk or Knudsen diffusion through the pore of the catalyst to the catalytic surface of the catalyst sites (metal particles).
3) Adsorption of A onto the catalytic surface of the catalyst sites.
4) Reaction of A to B on the catalytic sites.
5) Desorption of B from the surface.
6) Diffusion of B through the pore to the pore mouth.
7) Bulk diffusion of B from the external catalyst surface.

2.1.2 Monometallic versus Bimetallic

Another way of grouping the catalyst types is by the number of metal element that is anchored on the support. A monometallic catalyst comprises of a single metal element as the active component whereas a bimetallic catalyst comprise of two different metal elements.

The electronic and chemical properties of bimetallic catalysts are often different from those of their parent metals (Yu, Porosoff and Chen, 2012). For instance, Chen and Schmidt (1979) have found that the combination of palladium and platinum made them resistant against vaporisation. Otherwise, platinum alone is more exposed to vaporisation which can result in diminished activity. Long *et al.* (2011) explained that this difference in catalytic behaviours was caused by the change in configuration and electronic structure of the metal crystallites upon addition of the second metal element.

Many studies have shown that bimetallic catalysts have better performance than monometallic catalysts. In the field of catalytic combustion of methane, bimetallic palladium catalysts have been shown to have a stabilised activity (Yamamoto and Uchida, 1998; Narui *et al.*, 1999), to elevate the level of activity (Ahlström-Silversand and Odenbrand, 1997), and to improve the resistance against sulphur poisoning (Reyes *et al.*, 2000). Since catalytic oxidation of methane is an essential process of coal-fired power plant, an improved catalyst not only reduces energy required to ignite the fuel but also minimises the formation of unreacted hydrocarbons, nitrogen oxides and carbon monoxide (Persson, 2006).

Persson, Jansson, and Järås (2007), in particular, have compared the catalytic combustion of methane using monometallic Pd/Al_2O_3 and bimetallic $Pd\text{-}Pt/Al_2O_3$ as the catalyst. For the combustion of methane, palladium-based catalysts are used because of its ability to transform reversibly between PdO-Pd which gives rise to temperature self-control (Forzatti, 2003). The author mentioned that PdO is the active phase whereas elemental Pd is the inactive phase. Persson, Jansson, and Järås (2007) found that the activity of Pd/Al_2O_3 in methane combustion decreased with

time but the activity of Pd-Pt/Al_2O_3 increased slightly with time instead. They determined that Pt promoted the reduction of PdO, resulting in a higher rate of oxidation of methane. Another factor that caused Pd/Al_2O_3 to have lower activity was due to sintering (Narui *et al.*, 1999). Based on the research done by Narui *et al.* (1999), Pd catalyst displayed higher particle growth than its bimetallic counterpart, resulting in a loss of dispersion. Nevertheless, Araya *et al.* (2005) claimed that the loss of dispersion was insignificant. On the other hand, Roth *et al.*(2000) stated that the loss of activity of Pd/Al_2O_3 was a result of the creation of a low activity species, $Pd(OH)_2$.

In the food processing industry, hydrogenation is carried out to convert unsaturated fatty acids to saturated fatty acids. However, the hydrogenation process does not fully saturate the carbon-carbon double bonds of the fatty acids. Besides, unsaturated fatty acids tend to isomerise from a cis-configuration to a trans-configuration (Stankovic *et al.*, 2009). Singh *et al.* (2009) have proven that the consumption of trans fatty acids is bad for health. In the light of this issue, bimetallic catalysts have been studied and proven to outperform monometallic catalysts in this hydrogenation reaction (Alshaibani *et al.*, 2013; Shafii *et al.*, 2012). Alshaibani *et al.* (2013) compared hydrogenation conversion and selectivity to trans fatty acids in sunflower oil between Pd/Al_2O_3 catalyst and Pd-B/Al_2O_3 catalyst. It was determined that the Pd-B/Al_2O_3 catalyst gave higher conversion and lower selectivity compared to trans fatty acids. The same result is agreed by the research done by Shafii *et al.* (2012) who compared between Pd/Al_2O_3 catalyst and Pd-Pt/Al_2O_3 catalyst in hydrogenating palm oil.

2.2 Catalyst Preparation Overview

Nowadays, there is a vast array of methods of catalyst preparation. The catalytic properties are very dependent on the method by which the catalyst is synthesised. Basically, there are two important steps in preparing a supported catalyst:

a) Deposition of metal precursors on catalyst support
b) Heat treatment of catalyst

In this section, different ways of depositing metal precursors on catalyst support were presented, followed by description on heat treatment. An overview of the methods is illustrated in Figure 2.2

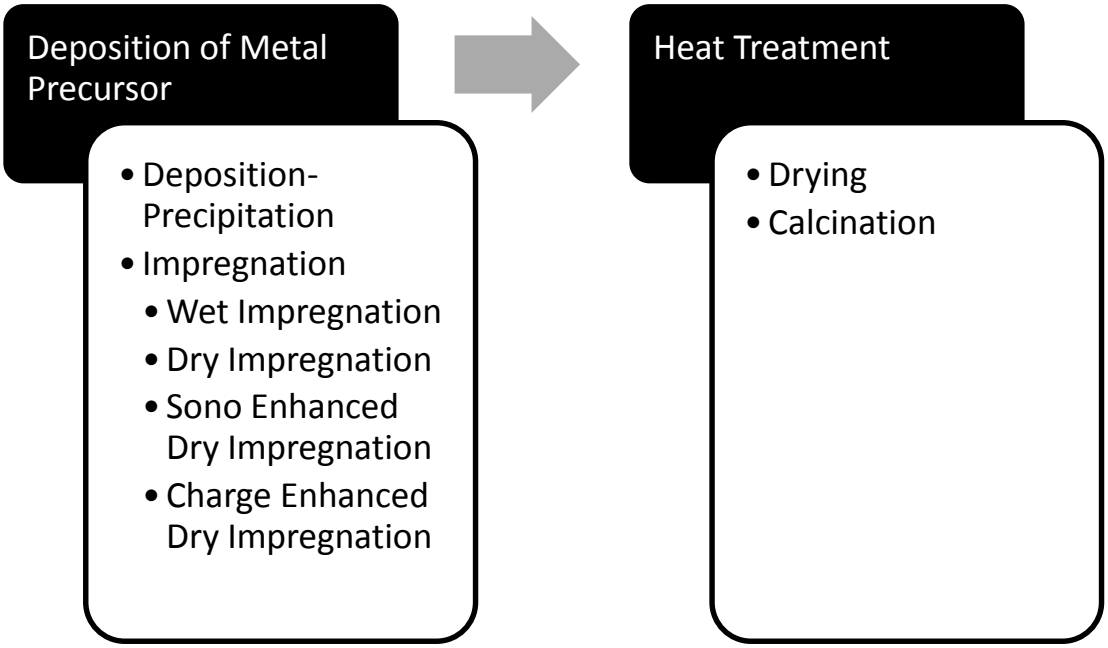

Figure 2.2: Catalyst Preparation Overview

2.2.1 Deposition-Precipitation

Deposition is a phenomenon whereby metal precursor such as hexachloroplatinate (CPA), $[PtCl_6]^{-2}$ and platinum tetraamine (PTA), $[(NH_3)_4Pt]^{+2}$ adsorbs or anchors on to an already produced support such as alumina or silica. Precipitation is the preparation of support precursors and metal precursors by mixing two or more solutions in a suitable method (Haber, 1991). Deposition-precipitation is the combined version of both deposition and precipitation. In this method, the support is suspended into a solution that contains soluble metal precursors. It involves the precipitation of metal precursors from bulk solutions and interaction with the support

surface (Campanati, Fornasari and Vaccari, 2003). Often, deposition-precipitation can achieve high metal loadings easily (Regalbuto, 2007). For example, Babu *et al.* (2009) prepared alumina supported Pd-Fe bimetallic catalysts by suspending alumina support in a mixture of aqueous solutions of $PdCl_2$ and $Fe(NO_3)_3$, which were the metal precursors of Pd and Fe respectively. They then brought about precipitation of the metal precursors exclusively on the support by changing the pH.

Precipitation is initiated by supersaturation, followed by nucleation and growth (Perego and Villa, 1997). Figure 2.3 shows the solubility curve as a function of temperature, pH and concentration.

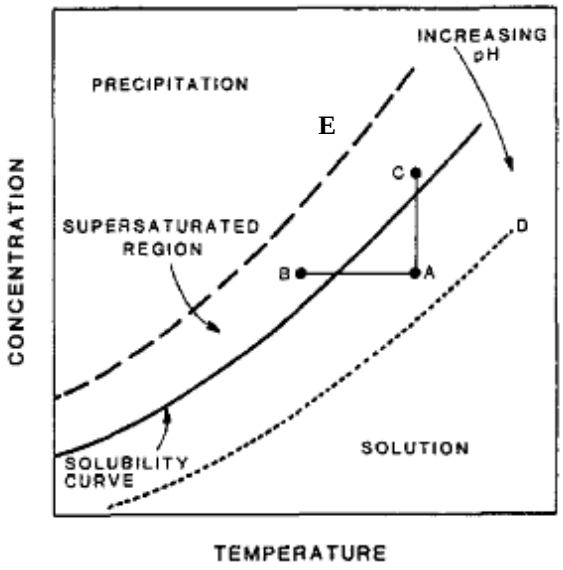

Figure 2.3: Solubility Curve of Metal Precursor as a Function of Concentration, Temperature and pH (Perego and Villa, 1997).

As shown in Figure 2.3, precipitation occurs when the system is in the unstable supersaturated region. For instance, Perego and Villa (1997) stated that supersaturated can be reached by changing the temperature (from A to B), evaporating the solvent to alter the concentration of solution (from A to C) or adding bases or acids to change the pH (alternate between line E and D). The solid precursor that has been precipitated then undergoes nucleation and growth.

It is desired that the metal precursors precipitate on support surface and not in bulk solution. Regalbuto (2007) explained that the addition of precipitating agent should be slow so that precipitates will not nucleate rapidly in the bulk solution. One such method is to employ hydrolysis of urea to increase the concentration of OH^- rather than to use normal alkali (Campanati, Fornasari and Vaccari, 2003). This is because urea is able to release OH^- gradually in the bulk solution (Campanati, Fornasari and Vaccari, 2003). According to Hermans and Geus (1979), the concentration of the solution must be kept in between the supersolubility curve of metal precursor in the presence of a support (line $SS_{support}$ in Figure 2.4) and the supersolubility curve of metal precursor in bulk solution (line *SS* in Figure 2.4). This is to ensure that the precursors only precipitate onto the support.

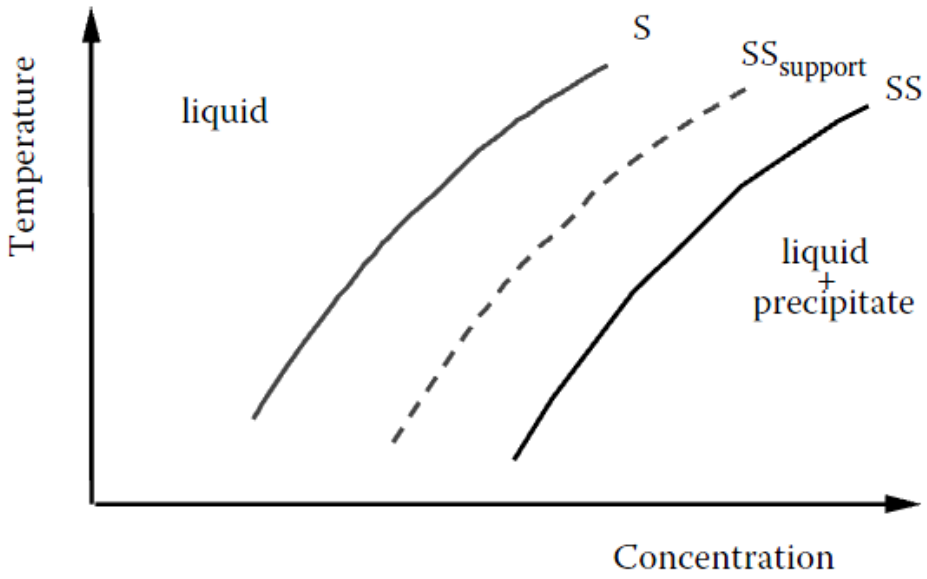

Figure 2.4: Schematic Phase Diagram for a Precipitate in Equilibrium with Its Solution and the Solid Support; (*S*) Solubility Curve

Besides changing pH, concentration and temperature, de Jong (2009) discussed about reduction deposition precipitation (RDP) and ligand removal as a method to bring about precipitation. RDP has been studied extensively by de Jong and Geus (1982). In RDP, the support is suspended in a solution containing the metal precursor and a reducing agent. This method is preferably used to deposit noble

metals due to their ease of reduction from aqueous solutions (de Jong and Geus, 1982).

2.2.2 Impregnation

Impregnation is a catalyst preparation procedure that is by far the simplest and probably most effective. In impregnation, the desired metallic elements to be adsorbed onto support are firstly obtained as metal precursors in solution. The solid support is then contacted with a specific volume of this metal-containing solution. In general, impregnation can be categorised into two major groups: wet impregnation (WI) and dry impregnation (DI) which is also known as incipient wetness method.

a) Wet Impregnation (WI)

For WI, the impregnating solution is in excess as compared to the pore volume of the support. The support is soaked in the impregnation solution for several hours or days to allow deposition of metal precursors on the support to happen (Haber, Block and Delmon, 1995). The duration of deposition takes a longer time as compared to DI because impregnating solution is drawn inwards to the pores of the support by slow diffusion process, rather than by capillary action as in the case of DI. Although the support is better mixed with the solution, filtration is needed to filter away the excess solution as well as those unadsorbed metal precursors. Therefore, the metal loading does not correspond to the amount of the metal precursor in the impregnating solution. Nevertheless, this method allows good control of metal particles distribution and high dispersion can be achieved (Haber, Block and Delmon, 1995).

b) Dry Impregnation (DI)

On the contrary, the impregnating solution required by DI is in just the right amount to fill the entire pore volume of the support. The impregnating solution is often sprayed or added dropwise to the support. DI has the advantages of avoiding filtration, minimising solution requirement and depositing a known metal loading onto the support. However, precursor-support interaction might be absent, giving rise to agglomeration of metal complexes (Regalbuto, 2007). It is to be noted that in normal dry impregnation method, charging of the catalyst surface is not of concern. This is the major difference from charge enhanced dry impregnation (CEDI) which is another similar method that will be presented in Section 2.2.2 (d). Figure 2.5 shows the different preparation mechanisms of (A) wet impregnation and (B) dry impregnation.

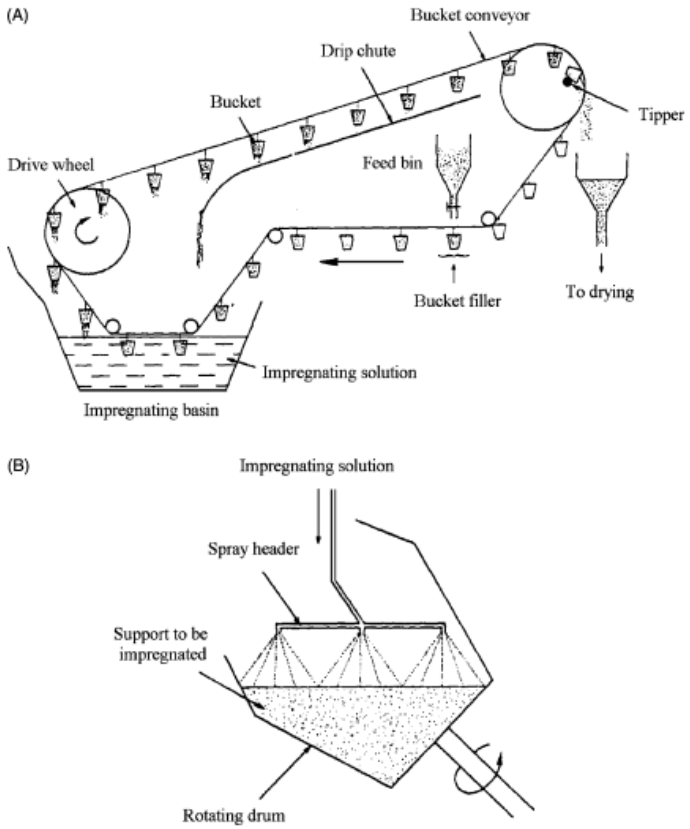

Figure 2.5: Impregnation Mechanisms: (A) Wet Impregnation (B) Dry Impregnation (Campanati, Fornasari and Vaccari, 2003).

c) Sono-enhanced Impregnation

Sono-enhanced impregnation or sonochemical impregnation uses ultrasonic waves with frequency ranges from 20 kHz to 10 MHz to impregnate nanosized metal particles on solid supports with high dispersion. Acoustic cavitation is introduced when the impregnating solution is irradiated with ultrasonic vibration. Acoustic cavitation involves the creation, growth, and sudden collapse of bubbles in a liquid (Ruan *et al.*, 2009). When ultrasound passes through a liquid, it creates a discontinuity in the liquid by introducing expansion waves and compression waves. The sound energy is carried by the bubbles. Bubbles either oscillate around their equilibrium position or grow in size and ultimately collapse abruptly. Their abrupt collapse causes immense release of heat and high pressure as well as increment of heating or cooling rates to a localised spot in the liquid (Suslick, 2000).

Many studies have shown that sonication is able to produce nanosized metal particles that are highly dispersed. One of the studies is the preparation of bimetallic Pd-Sn nanoparticles by (Jun, Lee, Kim and Kim, 2009). The authors applied sono-enhanced impregnation which resulted in Pd-Sn nanoparticles with the average size of 3 to 5 nm. Suslick (2000) attributed the formation of nanosized metal particles to the high cooling rate. He stated that the high cooling rate has prevented metal particles from crystallising. This statement was also agreed by Radziuk, Möhwald and Shchukin (2008). Toukoniitty *et al.*(2005), however, suggested that the formation of nanoparticles was due to the elevation of momentum of nanoparticles brought about by the shock waves from the collapse of bubbles. With this high momentum, metal particles collide violently and are fractured upon collisions, resulting in a diminished average particle size (Gogate and Kabadi, 2009). The momentum also prevents metal particles from getting aggregated as their van der Waals forces have been overcome (Vinodgopal *et al.*, 2010).

Perkas *et al.* (2014) have shown that catalysts synthesized by sono-enhanced method display higher activity than those prepared by dry impregnation method. Aside from having high dispersion, the increase in activity was attributed to the increase in pore size of the support. The microjets and shock waves from acoustic

cavitation generate mesopores on the support surface. Metal particles can then be adsorbed on the newly created pores, increasing the number of surface atoms.

d) Charge enhanced Dry Impregnation (CEDI)

Charge enhanced dry impregnation (CEDI) method distinguishes itself from dry impregnation (DI) by the need to charge the surface of catalyst support before impregnation. In other words, impregnation is induced by manipulating the pH level of the impregnating solution. CEDI method is the main highlight in this report. Unlike conventional DI, the metal precursor-support interactions using CEDI method can be controlled using strong electrostatic adsorption (SEA) mechanism (Regalbuto, 2007). SEA leads to a monolayer of metal precursor adsorbed on the support (de Jong, 2009). As a result, high dispersion of metal nanoparticles can be obtained.

Most solid catalyst supports are in the form of oxide and the surface of these oxides terminates with hydroxyl groups. The hydroxyl groups can be protonated or deprotonated depending on the pH of the impregnating solution and the nature of the support. To allow the adsorption of metal precursors onto the surface, these hydroxyl groups have to be protonated or deprotonated depending on the charge of the metal precursors. Before going into details, it is best to define the term point of zero charge (PZC). PZC is the pH where there is no charge exchange between the hydroxyl groups on the support surface and the metal complexes in the impregnating solution. When the pH of impregnating solution is higher than PZC, the hydroxyl groups are deprotonated and become O^- groups. This allows the adsorption of cationic metal complexes like PTA, $[(NH_3)_4Pt]^{+2}$. On the other hand, when the pH of impregnating solution is lower than PZC, the hydroxyl groups are protonated and become OH_2^+ groups. This permits the adsorption of anionic metal complexes like chloroplatinic acid (CPA), $[PtCl_6]^{-2}$. Figure 2.6 illustrates this phenomenon.

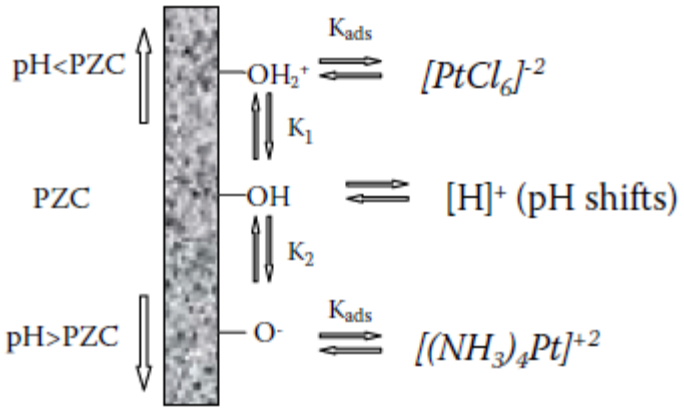

Figure 2.6: Schematic Diagram of Electrostatic Adsorption (Zhu *et al.*, 2013)

Different oxide supports have different PZCs. To adsorb the suitable metal precursors onto oxide support, the PZC of the support must be known in order to adjust the pH of the impregnating solution accordingly. Table 2.1 shows the PZC of some common oxide supports.

Table 2.1: PZC of Common Oxide Supports (Fierro, 2006)

Oxide Support	PZC
SiO_2	1.8
TiO_2	6.3
ZrO_2	6.7
γ-Al_2O_3	8.8
MgO	12.4

However, just by adjusting the pH according to the PZC is not enough to impregnate the metal precursors onto oxide supports. One must also consider the extent of proton transfer (Zhu *et al.*, 2013). Suppose there is a solution with a pH that is less than the PZC of a support but the pH is not far from it, the solution will not be able to effectively charge the hydroxyl groups even though the pH is less than the PZC. This is because there is insufficient amount of proton groups in the solution available to protonate the hydroxyl groups. Consequently, less protonated hydroxyl groups lead to less anions being adsorbed. If the initial pH is near to the PZC, the

final pH will converge to the PZC. This is known as the buffering capacity of the oxide surfaces (Park and Regalbuto, 1995). Figure 2.7 illustrates the above statement. In order to overcome the buffering capacity, the initial pH of the impregnating solution must be extremely basic or acidic. For instance, the optimal pH for the strongest platinum uptake for alumina support with a PZC of 8.8 ranges from 3 to 4 (Regalbuto, 2007)

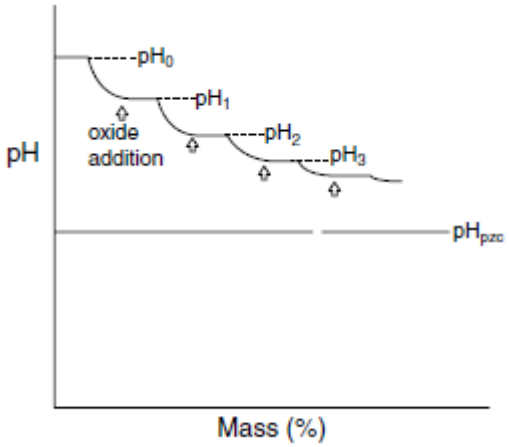

Figure 2.7: pH Shifts with Oxide Addition (Regalbuto, 2007)

Surface loading, *SL* (m^2/L) is defined as:

$$SL = \frac{m \times A}{V} \tag{2.1}$$

where

m = mass of oxide support, g

A = specific surface area of support, m^2/g

V = volume of impregnating solution, L

Regalbuto (2007) in their paper observed that the addition of oxides into the impregnating solution changes its pH. The higher the surface loading of the oxides, the higher is the change in pH. This implies that surface area of the oxide support can affect the protonation/deprotonation and therefore affect the metal uptake in the impregnating solution. It is thus necessary to first determine the PZC of the support

and then find out the initial pH of the impregnating solution that can give a final pH that is optimal for metal uptake.

2.2.3 Heat Treatment

After the metal precursors have anchored on the support, the catalysts undergo two stages of heat treatment to remove moisture and ligands. The product obtained is normally an oxide which can be stored conveniently. The first stage is drying and the second stage is calcination.

a) Drying

Drying removes impregnating solvent from the pores of the support. This results in higher concentration of precursor. The drying temperature usually ranges from 50 to 250 ^{o}C (Regalbuto, 2007), depending on the boiling point of the solvent. Drying can be done in an oven, fluidised bed dryer, spray dryer and freeze dryer (Haber, 1991). Koptyug *et al.*(2000) found out that the solvent is removed via capillary flow and diffusion. When solvent is removed from the pores, the metal precursors have the tendency to redistribute by adsorption/desorption (Neimark, Kheifets and Fenelonov, 1981). This happens when the metal precursors are not strongly attached to the solid support. The metal precursors can subsequently be removed from the pores if bubbles form and expand in the pores (Haber, Block and Delmon, 1995). Nevertheless, this problem can be solved by drying the catalyst gently at room temperature to allow the precursors to have enough time to diffuse back (Qin and Ramkrishna, 2005). Besides temperature, heating rate is also a factor that governs drying. In a research done by Komiyama, Merrill and Hansberger (1980) on Ni/Al_2O_3, the authors found that small nickel particles were well disseminated across alumina at a heating rate of 10 ^{o}C/min but were segregated at the mouth of pores when the heating rate was six-fold lower.

b) Calcination

Calcination is a term used specifically to describe heat treatment in air or oxygen (Haber, 1991). Unlike drying, calcination involves the chemical transformation of the precursor. It removes ligands, reduces the metal precursor to its active elemental state and stabilises mechanical properties (Campanati, Fornasari and Vaccari, 2003). For example, calcination removes chlorine and hydrogen from platinum-based catalyst prepared by chloroplatinic acid and turns the platinum into platinum oxide. Care should be taken in selecting the heating temperature and pressure so as to generate stable active phase and prevent sintering.

2.3 Impregnation Method for Bimetallic Catalysts

As mentioned earlier, there are two metal elements in a bimetallic catalyst. The impregnation method of the two metal elements can be divided into coimpregnation and sequential impregnation. In coimpregnation, two metal precursors are mixed before impregnating on the catalyst support. On the other hand, in sequential impregnation, the second metal precursor is impregnated only after the first metal precursor has been impregnated, dried and calcined on the catalyst support. The difference in impregnation method has great influence on the catalytic activity. In this section, the difference between coimpregnation and sequential impregnation is illustrated.

It has been reported that coimpregnation often leads to the formation of alloy of the two metals (Persson, Jansson and Järås, 2007; Bonarowska and Karpiński, 2008; Chantaravitoon, Chavadej and Schwank, 2004). In the case of sequential impregnation, the interaction between two metals is more complex. Some researchers found that a core-shell structure is formed, whereby the first metal to be impregnated is the core and the second metal is the shell (Cho and Regalbuto, 2015; Tao *et al.*, 2008). Long *et al.* (2011) found that aside from core-shell structure,

alloying was also observed at the interfaces of the core and the shell of sequentially impregnated Pd-Pt catalyst.

Chantaravitoon, Chavadej and Schwank (2004) compared between coimpregnated and sequentially impregnated Pt-Sn (Sn first) catalysts and found that coimpregnation method facilitated high platinum dispersions relative to sequential impregnation method. In contrast, Pt-Pd bimetallic catalyst prepared by sequential impregnation (Pt first) exhibited higher activity than that prepared by coimpregnation (Auvray and Olsson, 2015).

2.4 Characteristics of Catalyst

After discussing on the many means of preparing a supported catalyst, the characteristics of the prepared catalyst have to be specified. In this section, the characteristics of catalyst are presented. They are:

a) Specific surface area
b) Total pore volume
c) Pore size distribution
d) Particle size distribution
e) Dispersion
f) Reducibility

2.4.1 Specific Surface Area

Specific surface area is defined as the total surface area of the catalyst per unit mass of catalyst. It is normally expressed in m^2/g or cm^2/g. It is useful in determining the available surface area to anchor and disperse the metal particles for a catalytic reaction. The total surface area consists of the external and the internal surface areas.

According to Haber (1991), the roughness of the surfaces makes it hard to concisely define the external surface area. Therefore, the external surface area is normally taken as the area of the envelope surrounding the outer part of the catalysts. The internal surface area, on the other hand, is the total areas of the walls of the pores and cracks. To determine the specific surface area, nitrogen adsorption with the help of Brunauer-Emmett-Teller (BET) theory is usually applied. The BET equation is given by:

$$\frac{1}{W[(P_0/P)-1]} = \frac{1}{W_m K} + \frac{K-1}{W_m K}\left(\frac{P}{P_0}\right) \tag{2.2}$$

where

W = weight of nitrogen adsorbed, g

P/P_0 = relative pressure

W_m = weight of nitrogen as monolayer, g

K = BET constant

According to Equation 2.2, the slope (m) and intercept (c) are given

$$m = \frac{K-1}{W_m K} \tag{2.3}$$

$$C = \frac{1}{W_m K} \tag{2.4}$$

By solving the slope and intercept, the value of W_m can be found. The specific surface area, S (m^2/g) is then given by:

$$S = \frac{W_m N A_S}{Mw} \tag{2.5}$$

where

N = Avogadro's constant (6.023×10^{23})

A_s = Nitrogen cross sectional area (16.2 $Å^2$)

M = Molecular weight of nitrogen, g/mol

w = Weight of sample catalyst, g

2.4.2 Total Pore Volume

Many catalysts are porous. Porosity of a catalyst is related to its specific surface area. A catalyst with high porosity is a catalyst with high specific surface area. Porosity can be regarded as the ratio of the void volume to the bulk catalyst volume. In order to find porosity, total pore volume needs to be known. Total pore volume can also be determined by using nitrogen adsorption. According to Haber (1991), the amount of nitrogen adsorbed at a relative pressure close to unity is assumed to be the total pore volume. Hence, total pore volume, V_p (L) is given

$$V_P = \frac{P_a V_{ads} V_m}{RT} \tag{2.6}$$

where

V_{ads} = Volume of gaseous nitrogen adsorbed, L

V_m = Molar volume of liquid nitrogen, L/mol

P_a = Ambient pressure, atm

T = Ambient temperature, K

R = Gas constant, L·atm/(K·mol)

2.4.3 Pore Size Distribution

According to Haber (1991), pore size distribution is the distribution of pore volume versus pore size. Pores are classified based on their sizes:

(1) Macropores : Pore size > 50 nm

(2) Mesopores : 2 nm < Pore size < 50 nm

(3) Micropores : Pore size < 2 nm

Similarly, pore size distribution can be measured by nitrogen adsorption. The nitrogen adsorption isotherm gives information on the pore size distribution for micropores and mesopores but not macropores (Barroso-Bogeat *et al.*, 2014).

2.4.4 Particle Size Distribution

Particle size distribution is also an important measurement because particle size affects specific surface area which ultimately affects the activity of the catalyst. The size of each particle is typically measured using transmission electron microscopy (TEM). A beam of electrons is irradiated on the sample catalyst. The areas that do not transmit electrons appear as dark spots. These dark spots can then form the outline of metal particles and thus their sizes can be measured.

2.4.5 Dispersion

Dispersion is defined as the ratio of surface atoms to the total number of atoms. It is noted that dispersion is inversely proportional to the particle size. Hence, the smaller the size of particle, the higher the dispersion and the higher amount of surface metal atoms available for reaction. Dispersion can be measured using the method of selective chemisorption. A specific amount of molecule is used to selectively adsorb or react on the surface of the catalyst. This amount is then related to the number of surface atoms using a pre-determined chemisorption stoichiometry (Tengco *et al.*, 2014). Different metal atoms have their own suitable adsorbates. According to Leofanti *et al.* (1997) the suitable adsorbates for platinum and palladium in particular are H_2 and CO.

2.4.6 Reducibility

Reducibility is the ease for the metal oxide on supported catalyst to be reduced by flowing a carrier mixture of hydrogen and inert gas. Metal oxide that can be reduced at low temperature has high reducibility. Reducibility is dictated by the bond strength between the metal oxide and the support. Metal oxide with strong metal-support interaction needs high temperature to complete the reduction. Furthermore, the

reducibility of metal oxide also depends on the type and surface area of the support (Li, Hu and Hill, 2006), and metal loading (Li and Chen, 1995). Besides, it has been reported that the addition of noble metals as the second metallic element can improve reducibility (Loiha *et al.*, 2011).

2.5 Adsorption of Metal Precursor

The adsorption of metal precursors on oxide surfaces can be quantified using adsorption isotherm and surface ionization models. Both models are based on parameters found in experimental data by means of regression analysis. However, surface ionization models take solid-liquid interface into account and involve more parameters. On the other hand, adsorption isotherm models require less parameters and hence they are easier and more preferred.

2.5.1 Adsorption Isotherm

An adsorption isotherm model represents the amount of metal precursors on oxide surfaces as a function of concentration of the metal precursors in the impregnating solution.

Langmuir isotherm is the most popular adsorption isotherm model used due to its simplicity. The rate of adsorption is given by Morbidelli, Gavriilidis and Varma (2005):

$$\frac{dn}{dt} = k^{+}C(n_s - n) - k^{-}n \qquad (2.7)$$

where

n = surface concentration, μmol/g

t = time, s

k^{+} = adsorption rate constant, L/(mol s)

C = metal precursor concentration, mol/L

n_s = saturation capacity, μmol/g

k^- = desorption rate constant, s^{-1}

At equilibrium state, the transient term is set to zero, with rate of adsorption equals to the rate of desorption. Hence, the Langmuir isotherm is given by (Morbidelli, Gavriilidis and Varma, 2005):

$$\frac{n_e}{n_s} = \frac{KC_e}{1+KC_e} \tag{2.8}$$

where

n = amount of precursor adsorbed at equilibrium, μmol/g

C_e = solution concentration at equilibrium, mol/L

K = k^+/k^-

= equilibrium adsorption constant

There are several assumptions made in deriving Langmuir isotherm. It assumes that the surface is energetically uniform so that there are no interactions between adsorbed precursors on adjacent sites. Without these interactions, metal precursors have the same probability of adsorbing onto any sites regardless whether the adjacent site is occupied or not. Surface coverage does not affect the differential energy of adsorption. Moreover, it also assumes that the adsorbed precursors are localized onto definite points of attachment on the surface which means that each site on the surface can only accommodate one adsorbed precursor, giving rise to a monolayer.

Nevertheless, the Langmuir isotherm is applicable to solution with low concentration. If the concentration is high, precursors may be adsorbed on top of one another, forming multilayers. The Langmuir isotherm model no longer works in this situation, and BET theory can be used to describe this phenomenon.

2.5.2 Factors that Affect the Adsorption of Precursor

There are a variety of parameters that affect adsorption, namely pH of impregnating solution, the nature of support and surface heterogeneity.

The effect of pH has been discussed earlier in this report. In this section, the effect of pH is correlated with the nature of support. Heise and Schwarz (1985) suggest that decreasing pH of solution can cause alumina support to dissolve, leading to a decrease in the amount of adsorption sites and adsorbed platinum. However, Shah and Regalbuto (1994) claim that increased ionic strength is the real cause instead. When more and more negative charges are built up, a "double layer compression" or "electric screening" prevents the metal precursors from getting into contact. The electric screening is also seen when the pH is extremely high. Figure 2.8 illustrates the volcano-shaped curve of the metal uptake with both extremes of pH showing poor metal uptake.

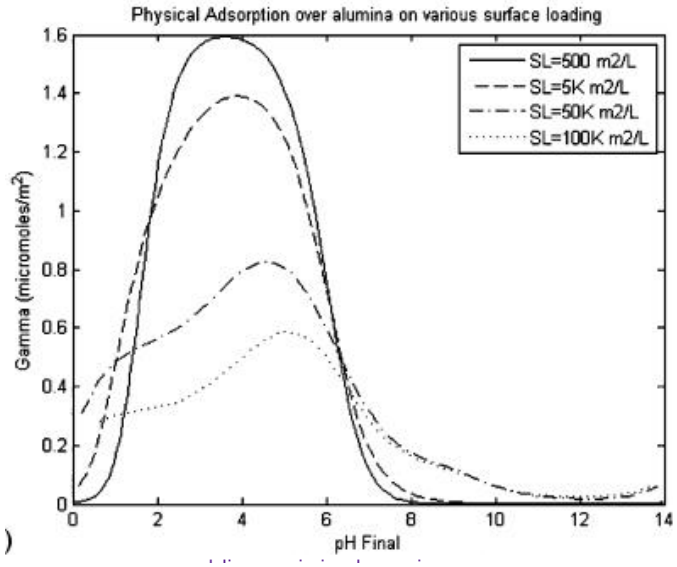

Figure 2.8: Metal Uptake by Alumina against Final pH (Zhu *et al.*, 2013)

Furthermore, contrary to the theory explained in Section 2.2.2 (d), some cations might adsorb on support even though the pH of impregnating solution is higher than the PZC and some anions might adsorb on support even though the pH is lower than the PZC. Experimental data obtained by Hohl and Stumm (1976) and Komiyama *et al.* (1980) have demonstrated this peculiarity. This behaviour is attributed to the existence of different species of sites whereby each of them has different affinities for the metal precursors (Abello *et al.*, 1995). Another explanation was given by Wang and Hall (1982). They claimed that surface heterogeneity was the result of the existence of different crystal planes of alumina whereby their isoelectric points are distinct from one another.

CHAPTER 3

METHODOLOGY

3.1 Materials

The metal oxide support employed was spherical γ-alumina pellets from Zibo Wufeng Aluminium Magnesium Technology Co. Ltd. The physicochemical properties of γ-alumina were provided by the supplier and are shown in Table 3.1.

The precursor for platinum was chloroplatinic acid (CPA) (37.5 wt%) while the precursor for palladium was palladium chloride ($PdCl_2$) (59.5 wt%). Both of them were obtained from Yurui (Shanghai) Chemical Co. Ltd. CPA solution was prepared by dissolving CPA solids with deionised water. $PdCl_2$ is hardly soluble in water and thus $PdCl_2$ solution was prepared by dissolving $PdCl_2$ solids with HCl.

Table 3.1: Physicochemical Properties of γ-Alumina

Composition of γ-Alumina Pellet				Bulk	Surface	Pore	Crush	Pellet
Al_2O_3	SiO_2	Fe_2O_3	Na_2O	Density	Area	Volume	Strength	Diameter
≥92 %	≤0.1 %	≤0.04 %	≤0.1 %	0.65 g/mL	≥200 m^2/g	≥0.42 mL/g	90 N	≈4 mm

3.2 Determination of Point of Zero Charge (PZC)

As mentioned in Section 2.2.2 (d), for charge enhanced dry impregnation to take place, the point of zero charge (PZC) of the γ-alumina pellet must be known. At this pH, the electrical charge density on the support surface is zero. The determination test was conducted by following the steps below:

a) The γ-alumina pellets were crushed using a pestle and mortar.
b) Deionised water solutions of various initial pHs were prepared using HCl and NaOH. pH measurement was done using CyberScan pH 510
c) Surface loading of alumina was fixed at 50 m^2/L. To achieve a surface loading of 50 m^2/L, 0.05 g of crushed γ-alumina powder was weighed and transferred to a beaker filled with 200 mL of the pH adjusted water solution (Calculation on surface loading is provided in Appendix A).
d) Step (c) was repeated by immersing 0.05 g of crushed γ-alumina powder in water solutions of other initial pHs.
e) The mixture was stirred for 8 minutes at room temperature.
f) The mixture was then allowed to stabilise without stirring for 10 minutes.
g) The final pH of the water solution was then recorded.
h) Steps (c) to (g) were repeated for surface loading of 500 m^2/L and 1000 m^2/L. It was done by changing the volume of solution while fixing the mass of crushed γ-alumina powder at 0.05 g. The purpose of varying the surface loading was to get a better picture of the location of PZC.
i) A graph of final pH versus initial pH was plotted.

3.3 Determination of pH for Optimal Adsorption

After knowing the PZC, it is also important to decide on the pH of impregnating solution that gives optimal adsorption of platinum and palladium. The adsorption survey was done by the steps listed below:

a) The γ-alumina pellets were crushed using a pestle and mortar.
b) 600 ppb of CPA solution was prepared over the pH range of 1 to 11 using HCl and NaOH. 50 mL of CPA solution was prepared for each pH.
c) 200 ppb of $PdCl_2$ was prepared over the pH range of 0.5 to 6 using HCl and NaOH. 50 mL of $PdCl_2$ solution was prepared for each pH.
d) 0.045 g of γ-alumina powder was weighed to obtain a surface loading of 600 m^2/L in 15 mL of solution.
e) Each γ-alumina powder was added to 15 mL of each pH adjusted CPA/$PdCl_2$ solution.
f) The mixture was mixed thoroughly for 1 hour.
g) Final pH values were measured.
h) The slurry solutions were filtered for final concentration measurement using inductively coupled plasma optical emission spectroscopy (ICP-OES, Perkin-Elmer Optima 7000 DV).
i) Initial solutions which were not contacted with γ-alumina, at each pH, were tested with ICP-OES to measure the initial concentration as well.
j) A graph of adsorption density versus final pH was plotted.

3.4 Preparation of Pd-Pt/Al_2O_3 Bimetallic Catalyst

Pd-Pt/Al_2O_3 bimetallic catalysts were prepared using charge-enhanced dry impregnation (CEDI) method. The calculated surface loading of alumina was as high as 444 444 m^2/L (Appendix A).

As demonstrated in Section 4.2, the pH for optimal adsorption of both CPA and $PdCl_2$ was found to be pH 3. It is reminded that this pH was the final pH of

impregnating solution after contact with alumina. Due to the buffering effect of alumina which tends to increase the pH of impregnating solution, especially in such a high surface loading (as described in Section 4.1), the starting pH of CPA and $PdCl_2$ solution was adjusted to around pH 0.5 using HCl.

Two sets of Pd-Pt/Al_2O_3 bimetallic catalysts were prepared. The first set was to find out the effect of atomic ratio of Pt:Pd on characteristics of catalyst. The second set was to find out the effect of impregnation method on characteristics of catalyst.

For the first set, coimpregnation of platinum and palladium on alumina support was carried out. CPA and $PdCl_2$ solutions were mixed into four different impregnating solutions with various atomic ratio of Pt:Pd. These premixed impregnating solutions were then adjusted to pH 0.5. (Detailed calculations on getting the right atomic ratio are reported in Appendix D). After that, the impregnating solution with an amount equal to the pore volume of the γ-alumina pellet was added dropwise to the pellet. The impregnation lasted for 2 hours. Subsequently, they underwent drying in the oven at 110 ^oC for 2 hours, followed by calcination at 500 ^oC for 5 hours in purified air using a tube furnace.

For the second set, a sample of Pd-Pt/Al_2O_3 bimetallic catalyst was prepared by sequential impregnation of CPA and $PdCl_2$. The preparation method was mostly similar to the abovementioned method with some exceptions. Rather than mixing CPA and $PdCl_2$ solutions, only $PdCl_2$ solution was first added dropwise to the pellet. The impregnation, drying and calcination parameters remained the same as those of coimpregnation. After calcination, Pd/Al_2O_3 was formed. CPA was then impregnated on Pd/Al_2O_3 using the same manner as the impregnation of $PdCl_2$. After the second calcination, Pd-Pt/Al_2O_3 bimetallic catalyst was formed. The catalyst designation was tabulated in Table 3.2.

A general denotation of Pd-Pt/Al_2O_3 is used to represent the palladium and platinum bimetallic catalyst supported on γ-alumina. The catalyst is further denoted as *X*Pt:*Y*Pd/Al_2O_3-Coimp for coimpregnated catalyst and *X*Pt:*Y*Pd/Al_2O_3-Seq for sequential impregnated catalyst. Here *X* and *Y* represent the nominal atomic ratio of

Pt:Pd. For example, 1Pt:1Pd/Al_2O_3-Seq denotes a sequential impregnated Pd-Pt/Al_2O_3 bimetallic catalyst with a 1:1 nominal atomic ratio of Pt:Pd. On the other hand, 0Pt:1Pd/Al_2O_3 denotes a Pd/Al_2O_3 monometallic catalyst.

Table 3.2: Catalyst Designation

Catalyst Name	Metal Loading (wt%)[a]		Nominal Atomic Ratio	
	Pt	Pd	Pt	Pd
0Pt:1Pd/Al_2O_3	0.00	0.43	0	1
1Pt:0Pd/Al_2O_3	1.56	0.00	1	0
4Pt:1Pd/Al_2O_3-Coimp	2.13	0.29	4	1
1Pt:1Pd/Al_2O_3-Coimp	0.79	0.29	1	1
1Pt:1Pd/Al_2O_3-Seq	0.79	0.29	1	1

[a]Determined by ICP-OES

3.5 Catalyst Characterisation

After preparing the catalyst samples, they were sent for a series of characterisation tests to determine their performance. The characterisation tests were X-ray diffraction (XRD), temperature programmed reduction (TPR), scanning electron microscopy (SEM) and energy-dispersive X-ray spectroscopy (EDXS)

3.5.1 X-ray Diffraction (XRD) Characterisation

X-ray diffraction (XRD) studies were carried out to investigate the phase of catalyst samples. The analysis employed a Shimadzu LabX XRD-6000 diffractometer with Cu Kα radiation (λ = 1.54 Å) operated at 40 kV and 30 mA. Catalyst samples were crushed to powder and mounted on the sample holder beforehand. They were scanned from 10^o to 80^o with a scan rate of 2^o/min.

3.5.2 Temperature Programmed Reduction (TPR) Characterisation

Temperature programmed reduction (TPR) studies were conducted to determine the reducibility of catalyst, i.e. the reduction temperature. Each peak in the TPR spectra represents the presence of oxide species. Thermo Scientific TPDRO 1100 with a thermal conductivity detector (TCD) was used to detect the amount of consumption of hydrogen from the carrier mixture. The catalysts samples were crushed beforehand. For each run, the sampling size was 0.02 g. Before analysis, the samples were purged with 25 mL/min pure hydrogen to remove moisture. Purging started from room temperature to 110 ^{o}C at a heating ramp of 5 ^{o}C/min and held for 1 hour. For analysis, the flowing gas was 5 vol% H_2/N_2 and the flowrate was 25 mL/min. Temperature increased from room temperature to 500 ^{o}C with a heating ramp of 5 ^{o}C/min.

3.5.3 Scanning Electron Microscopy (SEM) and Energy-dispersive X-ray Spectroscopy (EDXS)

Scanning electron microscopy (SEM) was used to obtain images of alumina support before impregnation with a Hitachi S-3400N at 15 kV, 6.2 mm working distance, and ×5000 magnification. The alumina support was coated with palladium and gold using Emitech Sputter Coater to increase its conductivity.

Since Hitachi S-3400N could not image metal nanoparticles in catalyst samples, field emission scanning electron microscopy (FESEM) was used instead. The FESEM machine was a JEOL JSM-6701F. Images of nanoparticles were taken at 2 kV, 6.1 mm working distance, and ×30 000 magnification. The elemental composition of nanoparticles was determined by energy-dispersive X-ray spectroscopy (EDXS) using the same machine. The catalyst samples were crushed to powder and coated with platinum before analysis using a JEOL JFC-1600 Sputter Coater.

CHAPTER 4

RESULTS AND DISCUSSION

4.1 Determination of Point of Zero Charge (PZC)

The results from the determination of point of zero charge (PZC) are shown in Figure 4.1 below. For every surface loading, there is a plateau occurring in the range between pH 7 and pH 8.5. The readings of final pH are averaged out for all surface loadings, resulting in an averaged plateau occurring at pH 7.8. This pH is regarded as the PZC of the γ-alumina pellet. This is almost in well accordance with several authors who found that the range of PZC of alumina was in between pH 8.0 to pH 9.3 (Feltes and Timmons, n.d.; Park and Regalbuto, 1995; Spieker and Regalbuto, 2001).

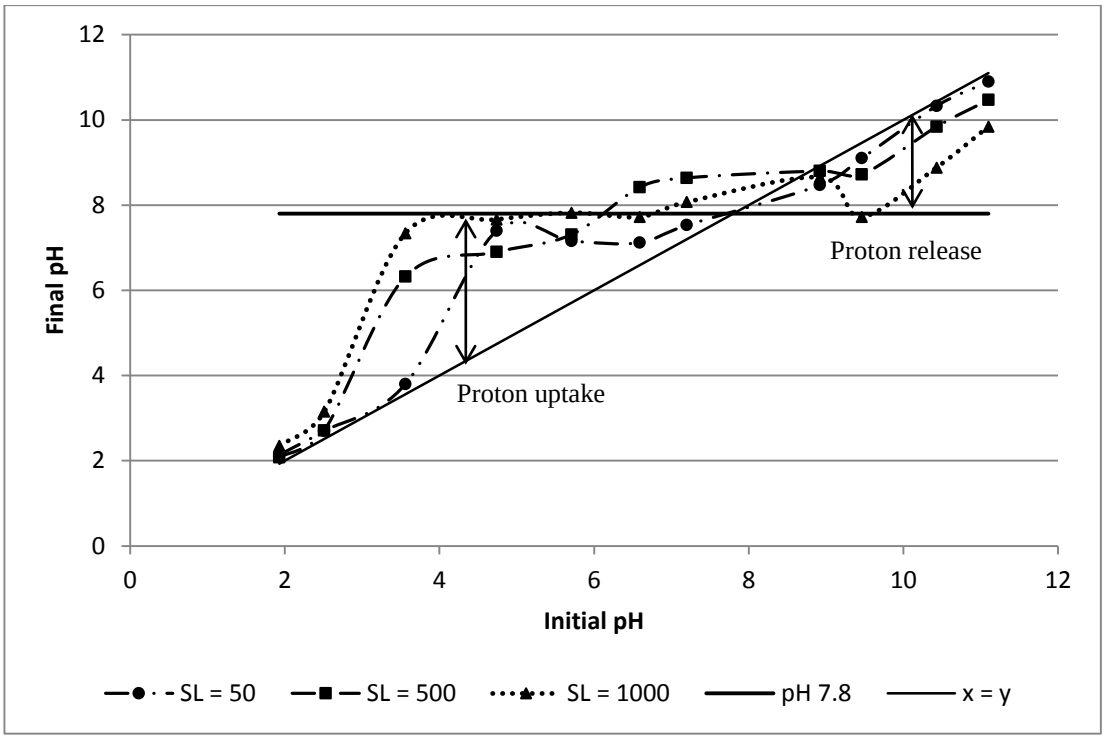

Figure 4.1: Equilibrium pH for γ-Alumina at Different Surface Loadings (m^2/L)

Besides, there are pH shifts occurring below and above the PZC. Initial pH below the PZC shifts to higher pH whereas initial pH above the PZC shifts to lower pH. If there is no pH shifts, the points in Figure 4.1 would fall on the "x=y" line. pH shifts are attributed to the surface oxide charging and buffering effect of the alumina (Regalbuto, 2007). As discussed previously, when the pH is below the PZC, the hydroxyl groups on the surface of alumina are protonated (aka proton uptake). The bulk pH then increases. On the contrary, when the pH is above the PZC, the hydroxyl groups are deprotonated (aka proton release) and so the bulk pH decreases. This buffering effect tends to bring the final pH towards the PZC.

The buffering effect is more obvious when the oxide surface loading is higher. As shown by Figure 4.1, the plateau is wider at higher surface loading. This result has been pointed out by Park and Regalbuto (1995) before. At high surface loading, hydroxyl groups on the oxide surface far outnumber protons and hydroxides in the bulk solution. More protons and hydroxides are required to protonate and deprotonate the hydroxyl groups. Therefore, at higher surface loading, the initial pH shifts greatly towards the PZC as indicated by a steeper slope. Thus, one could

expect that the final pH of the bulk solution will almost always be in the PZC in the case of dry impregnation whereby the surface loading is very high (Regalbuto, 2007; Zhu, Cho, Pasupong and Regalbuto, 2013).

One interesting trend depicted by Figure 4.1 is that the pH shifts are less prominent at pH extremes (pH 2 and pH 11). The final pH is similar to the initial pH, as shown by its proximity to the "x=y" line. This is because the number of protons and hydroxides in the bulk solution is a lot more than the number of hydroxyl groups on the oxide surface. Even after protonation and deprotonation with the hydroxyl groups, there are still many protons and hydroxides in the bulk solution. The buffering effect is diminished and the oxide surface is said to be significantly charged (Regalbuto, 2007). In a nutshell, for charge-enhanced dry impregnation, the pH of the bulk solution must be made extremely acidic or alkaline in order to charge the oxide surface and allow metal precursor-support interaction to take place.

In the case of this thesis, the surface loading is 444 444 m^2/L. Due to the fact that there was no spear-tip pH meter available, the surface loading had to be lowered in order to have at least 2 mL of bulk solution to be tested for its final pH. Therefore, Figure 4.1 only showed oxide surface loading of 50 m^2/L, 500 m^2/L and 1000 m^2/L. Despite of this limitation, Figure 4.1 has provided a great way to expect what the starting pH should be in order to get a very low or very high final pH, away from the PZC.

In summary, the PZC of γ-alumina is found to be at around pH 7.8. The initial pH of bulk solution must be highly acidic or alkaline so that the final pH will not shift to the PZC. This is even more so for higher surface loading whereby the buffering capacity of oxide is greater. Nevertheless, extreme pH does not necessarily reinforce metal precursor-support interaction and maximise metal uptake by the alumina support. In the next section, an adsorption survey was performed to find out the effect of pH on metal uptake.

4.2 Determination of pH for Optimal Adsorption

Results of the adsorption of metal precursors (CPA and $PdCl_2$) on alumina support versus final pH are shown in Figure 4.2. According to Figure 4.2, the maximum adsorption density of anionic chloroplatinic acid (CPA) is observed to be 0.53 nmol/m^2. On the other hand, the maximum adsorption density of anionic palladium chloride ($PdCl_2$) is 1.46 nmol/m^2. Both CPA and $PdCl_2$ exhibit maximum adsorption density at pH 3. This pH is below the PZC whereby the hydroxyl groups are protonated and become positively-charged where anionic CPA and $PdCl_2$ can electrostatically adsorb. Moreover, both adsorption patterns are volcano-shaped, which is normal for strong electrostatic adsorption (SEA) (Cho and Regalbuto, 2015). These data are in agreement with past reports (Zhu *et al.*, 2013; Cho and Regalbuto, 2015; Mang, Breitscheidel, Polanek and Knözinger, 1993). As pH moves further away from the PZC towards the acidic end, surface potential increases. Consequently, metal uptake increases too.

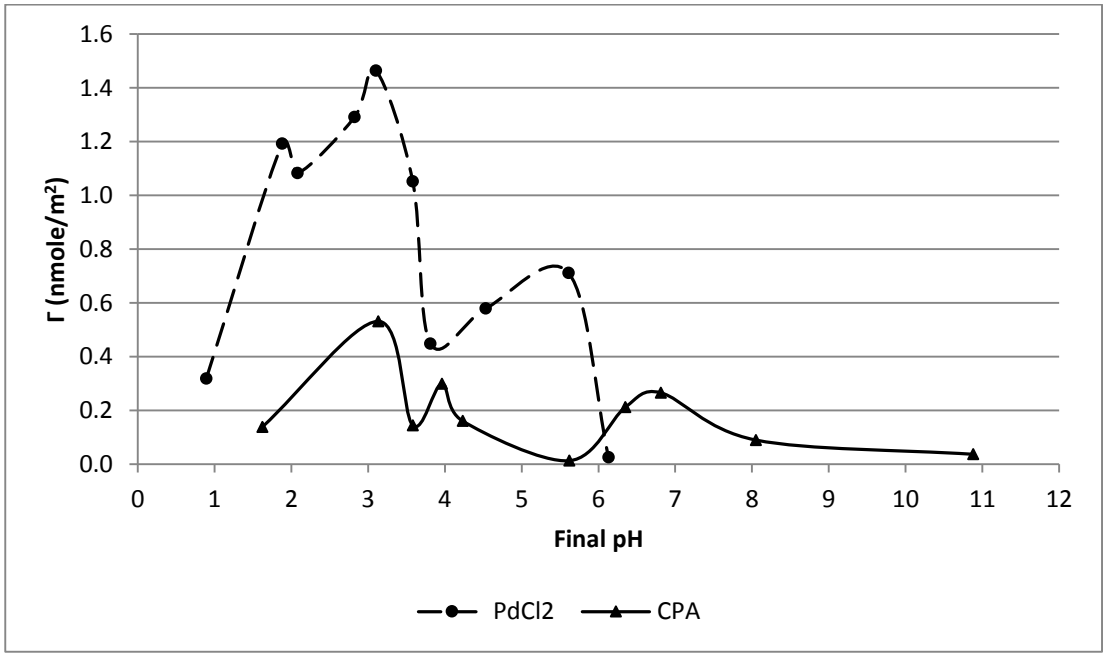

Figure 4.2: Uptake of Metal Precursors on Alumina Support

As highlighted previously, extreme pH does not guarantee a good metal precursor adsorption on catalyst support. This is clearly shown by Figure 4.2 whereby the adsorption of CPA and $PdCl_2$ plummets near pH 1. As mentioned in

Section 2.5.2, support dissolution and high ionic strength are the two possible causes for this phenomenon. Zhu *et al.* (2013) reported that dissolution of support is unlikely because the buffering effect possessed by the alumina support is able to quickly increase or lower the pH to levels at which the charge is high enough for SEA but mild enough so that there is no significant dissolution. Hence, the low metal uptake at pH 1 in Figure 4.2 can be better explained by the increase of ionic strength.

Besides, as pH moves from pH 3 to higher pH, metal adsorption density plummets again. This is because both CPA and $PdCl_2$ are anionic metal precursors and can only be adsorbed on positively-charged surface oxide. This uptake survey also confirms that the PZC is at pH 7.8 because the adsorption density is very little at that particular pH. Above the PZC, the surface oxide becomes negatively-charged and repulsion forces hinder adsorption of the anionic metal precursors.

After knowing that maximum adsorption density occurs at pH 3, Figure 4.1 was used to expect the pH that was required to start with in order to get to that pH 3. It was decided that the starting pH of impregnating solution was pH 0.5

4.3 Catalyst Characterisation

4.3.1 X-ray Diffraction (XRD) Characterisation

X-ray diffraction was used to investigate the phase of alumina support. The XRD pattern for the alumina support is given by Figure 4.3. The peaks are at $2\theta = 37.5°$, 46.0°, and 67.0°. These results are distinct for γ-alumina (Rozita, Brydson and Scott, 2010; Alshaibani, Yaakob, Alsobaai and Sahri, 2013) and further confirm that the alumina support was of gamma type. Unfortunately, subsequent characterisation of catalyst samples was not possible as the operation of XRD machine was forbidden. Due to this limitation, the phases of platinum and palladium after calcination were unknown in both monometallic and bimetallic samples. Nevertheless, in the following section, possible phases of palladium and platinum can be found using temperature programmed reduction (TPR) characterisation.

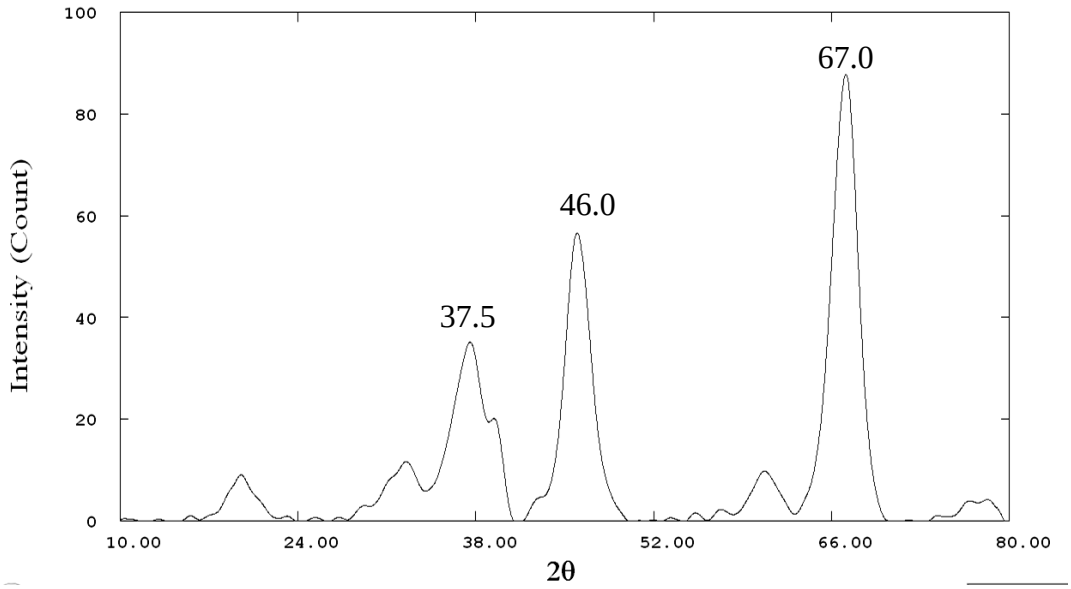

Figure 4.3: XRD Diffractogram for γ-Alumina

4.3.2 Temperature Programmed Reduction (TPR) Characterisation

Temperature programmed reduction (TPR) was used to evaluate the effect of metal ratio of Pt:Pd as well as the effect of impregnation method (coimpregnation or sequential impregnation) on the reducibility of alumina supported bimetallic Pd-Pt catalysts. Results of the TPR analysis to study the effect of atomic ratio of Pt:Pd are shown in Figure 4.4 and Figure 4.5. Monometallic Pt/Al_2O_3 and Pd/Al_2O_3 are shown for comparison purpose.

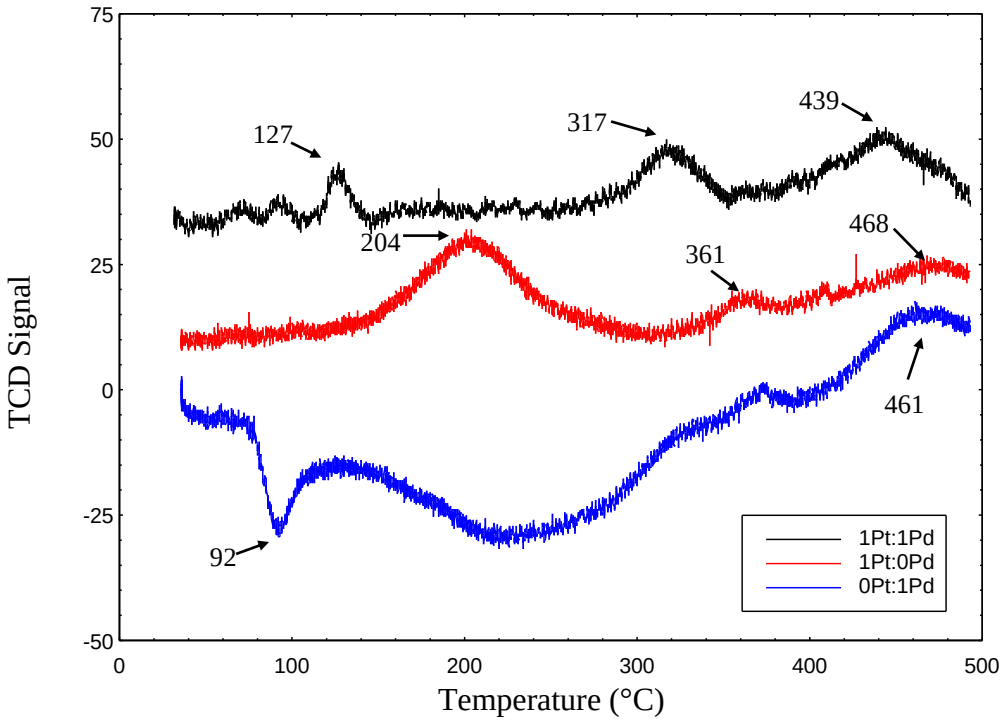

Figure 4.4: Temperature Programmed Reduction (TPR) Profiles of 1Pt:1Pd/Al_2O_3-Coimp, 1Pt:0Pd/Al_2O_3 and 0Pt:1Pd/Al_2O_3

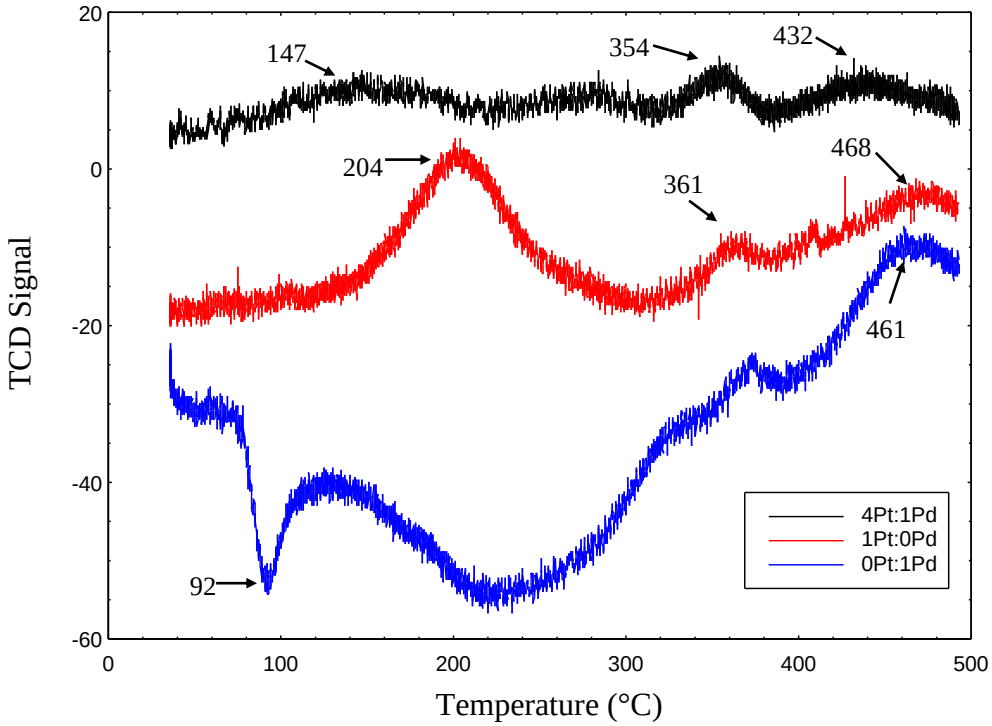

Figure 4.5: Temperature Programmed Reduction (TPR) Profiles of 4Pt:1Pd/Al_2O_3-Coimp, 1Pt:0Pd/Al_2O_3 and 0Pt:1Pd/Al_2O_3

According to the TPR profile of monometallic 0Pt:1Pd/Al_2O_3 catalyst, one can notice a drop in TCD signal at 92 ^oC which is attributed to hydrogen generation. This hydrogen release is due to decomposition of bulk palladium hydride formed when hydrogen diffused into the palladium particles (Lingaiah *et al.*, 2002; Amorim, Wang and Keane, 2011; Castellazzi, Groppi and Forzatti, 2010). The TPR spectrum of 0Pt:1Pd/Al_2O_3 in Figure 4.4 resembles the one done by Lieske and Volter (1985). The authors claimed that there are two kinds of PdO in the system. One of them is an easily reducible oxide which has a reduction peak at below the room temperature (not shown in Figure 4.4). The other is a more stable oxide which has interaction with the alumina, resulting in a high-temperature reduction peak at around 400 ^oC. Babu and co-workers (2009) found that the peak at 410 ^oC can be associated to the reduction of subsurface Pd species. The authors explained that formation of subsurface PdO phase is an indication of Pd being highly dispersed. Hence, the peak at 461 ^oC in Figure 4.4 could be attributed to this subsurface PdO.

In the case of monometallic 1Pt:0Pd/Al_2O_3 catalyst, there are three reduction peaks appearing at 204 ^oC, 361 ^oC and 468 ^oC. This suggests there are several species of platinum as mentioned by Jiang *et al.* (2007). Based on a study by Lieske, Lietz, Spindler and Volter (1983), the platinum species should exist in the form of PtO_xCl_y complex since the catalyst samples were impregnated with chloroplatinic acid precursor. Hwang and Yeh (1996) reported that there are two types of PtO_xCl_y complex, namely a three-dimensional bulk phase and a two-dimensional dispersive phase. According to them, a reduction peak at around 200 ^oC is characteristic of bulk PtO_xCl_y phase whereas a reduction peak at around 350 ^oC is distinct to a dispersive PtO_xCl_y phase whereby alumina support interacts strongly with platinum. Although this is not a strong evidence, this entails that the Pt/Al_2O_3 under study consisted of both bulk PtO_xCl_y phase and dispersive PtO_xCl_y phase.

By comparing bimetallic 4Pt:1Pd/Al_2O_3-Coimp (Figure 4.5) and 1Pt:1Pd/Al_2O_3-Coimp (Figure 4.4) with monometallic 1Pt:0Pd/Al_2O_3 and 0Pt:1Pd/Al_2O_3, one could notice that the locations of the reduction peaks of bimetallic catalysts are different from their monometallic counterparts. The reduction peaks are shifted to lower temperatures, proving that the interaction between platinum and palladium results in better reducibility. Noteworthy, the different

locations of reduction peaks might suggest that only bimetallic clusters were produced after reduction. However, Jiang *et al.* (2007) proposed that monometallic clusters might still be intact because they may be too small to give a reduction peak due to persistent interaction with nearby second metal atoms. Indeed Persson (2006) used transmission electron microscopy/energy-dispersive X-ray spectroscopy (TEM/EDXS) to confirm that bimetallic clusters (Pd-Pt alloy) and monometallic clusters (PdO) do coexist in particles of the bimetallic catalysts that have more than 50 at% palladium. The author also realised that the two domains are in close contact.

Furthermore, there is less intense hydride decomposition peak in the spectrum of 1Pt:1Pd/Al_2O_3-Coimp and totally no hydride decomposition peak for 4Pt:1Pd/Al_2O_3-Coimp as compared to 0Pt:1Pd/Al_2O_3. This suggests the addition of platinum has hindered the formation of palladium hydride. In fact, Bonarowska and Karpiński (2008) have evidenced that the appearance of palladium hydride decomposition peak is a great way to identify the degree of alloying between platinum and palladium in supported catalysts. They further clarified that a perfectly alloyed Pd-Pt catalyst should not show the hydride decomposition peak. Hence, it can be deduced platinum and palladium particles in 4Pt:1Pd/Al_2O_3-Coimp are better alloyed than 1Pt:1Pd/Al_2O_3-Coimp since the hydride decomposition peak is non-existent in 4Pt:1Pd/Al_2O_3-Coimp.

Moreover, it is observed that the reduction peaks of 4Pt:1Pd/Al_2O_3-Coimp (Figure 4.5) are broader than those of 1Pt:1Pd/Al_2O_3-Coimp (Figure 4.4). Table 4.1 shows the amount of hydrogen adsorbed in TPR analysis. It is observed that monometallic platinum has a higher amount of hydrogen adsorbed than monometallic palladium. Besides, the amount of hydrogen adsorbed by bimetallic catalysts is in between that by monometallic platinum and palladium, suggesting that the introduction of platinum increases hydrogen adsorption. The higher hydrogen adsorption in 4Pt:1Pd/Al_2O_3-Coimp can thus be explained by higher loading of platinum.

Table 4.1: Amount of Hydrogen Adsorbed in TPR Analysis

Catalyst	Amount of Hydrogen Adsorbed (μmol/g)
0Pt:1Pd/Al_2O_3	119.29
1Pt:0Pd/Al_2O_3	188.40
4Pt:1Pd/Al_2O_3-Coimp	134.82
1Pt:1Pd/Al_2O_3-Coimp	128.95
1Pt:1Pd/Al_2O_3-Seq	136.47

The reduction temperature of 4Pt:1Pd/Al_2O_3-Coimp is generally higher relative to 1Pt:1Pd/Al_2O_3-Coimp. This means that the metal-support interaction is stronger for 4Pt:1Pd/Al_2O_3-Coimp. This is inconsistent with previous studies (Ersson *et al.*, 2003; Strobel *et al.*, 2005; Persson, 2006). According to Persson (2006), platinum actually promotes PdO reduction.. The discrepancy might be due to small sampling size needed for TPR analysis, especially when the catalyst samples were not in the powder form in the first place.

Results of TPR analysis to study the effect of impregnation method are shown in Figure 4.6 and Figure 4.7. Similarly, monometallic 1Pt:0Pd/Al_2O_3 and 0Pt:1Pd/Al_2O_3 are shown for comparison purpose.

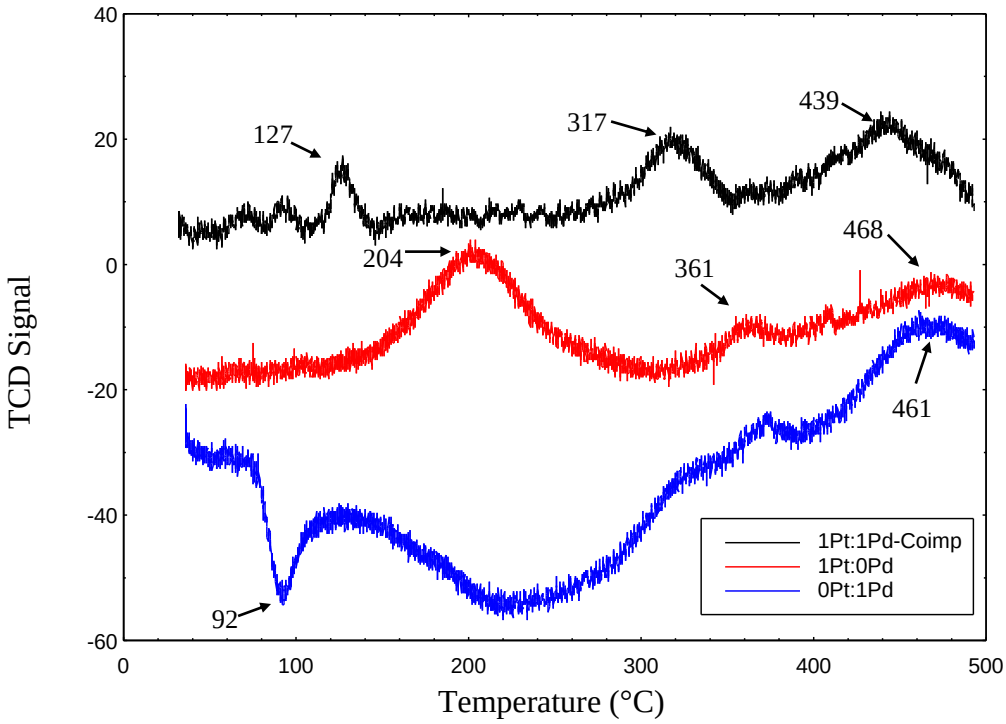

Figure 4.6: Temperature Programmed Reduction (TPR) Profiles of 1Pt:1Pd/Al_2O_3-Coimp, 1Pt:0Pd/Al_2O_3 and 0Pt:1Pd/Al_2O_3

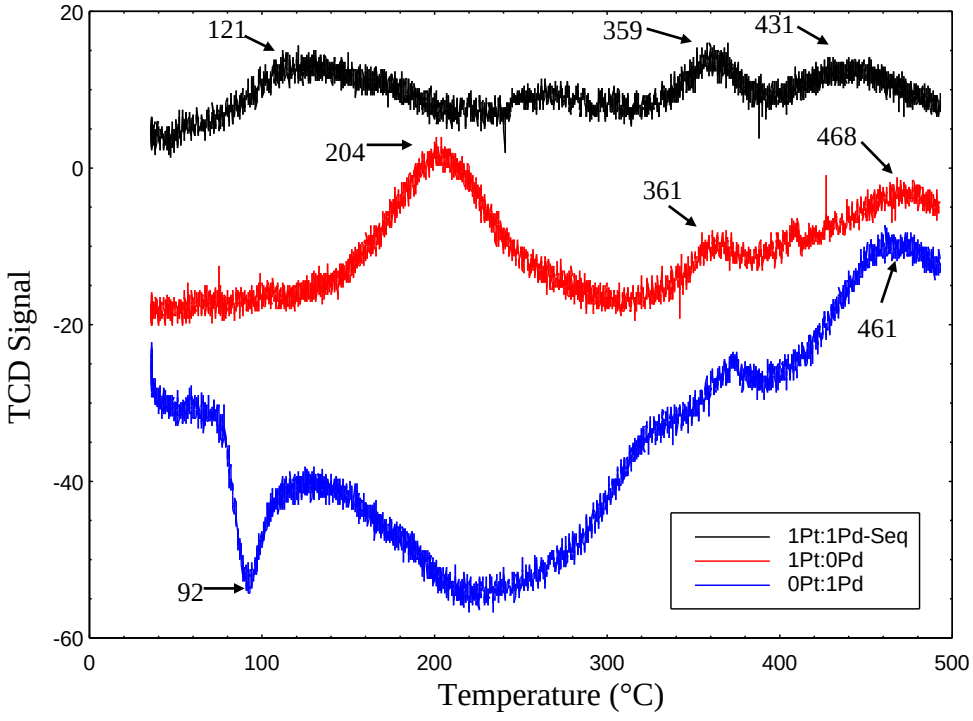

Figure 4.7: Temperature Programmed Reduction (TPR) Profiles of 1Pt:1Pd/Al_2O_3-Seq, 1Pt:0Pd/Al_2O_3 and 0Pt:1Pd/Al_2O_3

In overall, the reducibility of 1Pt:1Pd/Al_2O_3-Seq (Figure 4.7) is lower than that of 1Pt:1Pd/Al_2O_3-Coimp (Figure 4.6) since 1Pt:1Pd/Al_2O_3-Seq has higher-temperature peaks. This is an indication of a stronger metal-support interaction. Besides, according to Table 4.1, the amount of hydrogen adsorbed by 1Pt:1Pd/Al_2O_3-Seq is higher than that of 1Pt:1Pd/Al_2O_3-Coimp even though they both had the same metal loading. This might infer that 1Pt:1Pd/Al_2O_3-Seq has a core-shell structure. Since 1Pt:1Pd/Al_2O_3-Coimp which is comprised of Pd-Pt alloy structure has lower hydrogen adsorption than monometallic platinum (see Table 4.1), it implies that the platinum shell in 1Pt:1Pd/Al_2O_3-Seq was responsible for the higher hydrogen adsorption. Cho and Regalbuto (2015) have shown that coimpregnation of platinum and palladium yields Pd-Pt alloy whereas sequential impregnation of palladium followed by platinum yields a palladium core and platinum shell structure.

In summary, it is suggested that coimpregnated bimetallic Pd-Pt catalysts exist in an alloy of Pd-Pt. There are two reasons behind this. Firstly, reduction temperatures of bimetallic catalysts are different from their monometallic counterparts. Secondly, there is a diminished or absence of palladium hydride decomposition peak in bimetallic catalysts. Higher atomic ratio of Pt:Pd was found to have lower reducibility but higher amount of hydrogen adsorbed due to the higher amount of platinum in the Pd-Pt alloy. Furthermore, 1Pt:1Pd/Al_2O_3-Seq is likely to have a core-shell structure. Catalyst prepared by sequential impregnation has lower reducibility but higher hydrogen consumption than catalysts prepared by coimpregnation.

4.3.3 Scanning Electron Microscopy (SEM) and Energy-dispersive X-ray Spectroscopy (EDXS)

The morphology of alumina support prior to impregnation was studied using scanning electron microscopy (SEM). The particle size and dispersion of metal nanoparticles of Pd-Pt/Al_2O_3 catalyst were investigated using field emission scanning electron microscopy (FESEM) coupled with energy-dispersive X-ray spectroscopy (EDXS). Figure 4.8 shows the polycrystalline alumina support surface before

impregnation with platinum and palladium. It is observed that the surface is very rough.

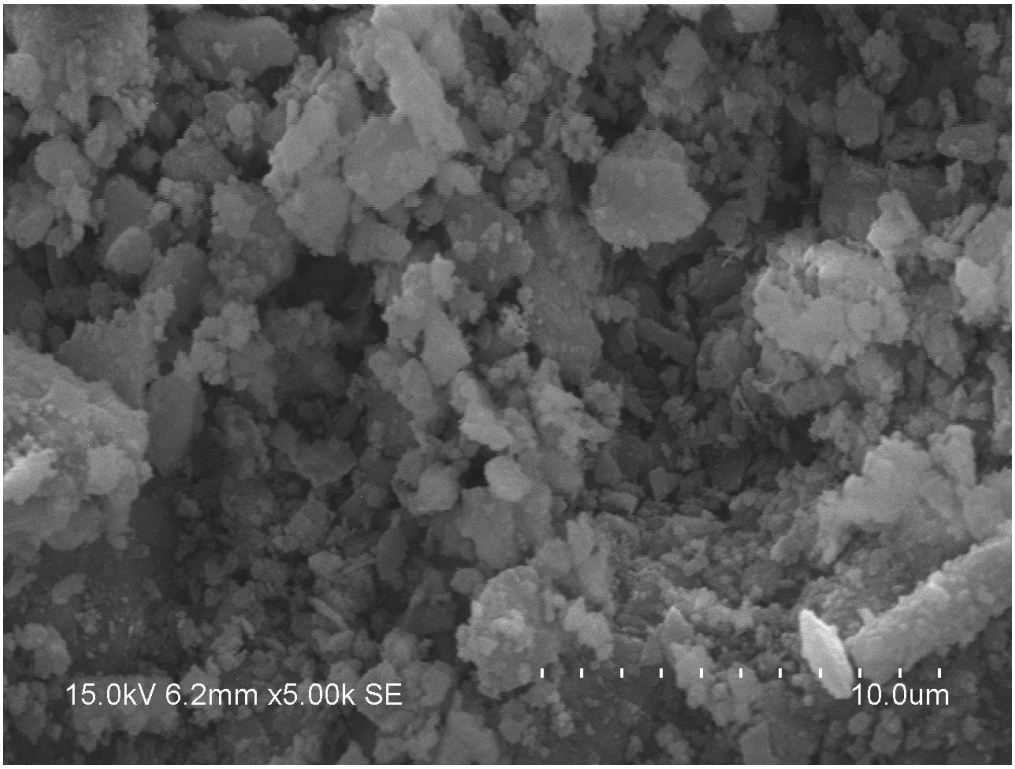

Figure 4.8: SEM Image of Alumina Support before Impregnation

Figure 4.9 (a) and Figure 4.9 (b) show the FESEM image of 1Pt:1Pd/Al_2O_3-Coimp and 4Pt:1Pd/Al_2O_3-Coimp respectively. Markers on the images represent the potential platinum and palladium particles that were adsorbed on alumina support. However, these particles could not be confirmed to be the exact representation of platinum and palladium because the catalyst samples could not be analysed by EDXS. This was due to the fact that the very coating metal used to coat the catalyst samples for FESEM imaging was platinum.

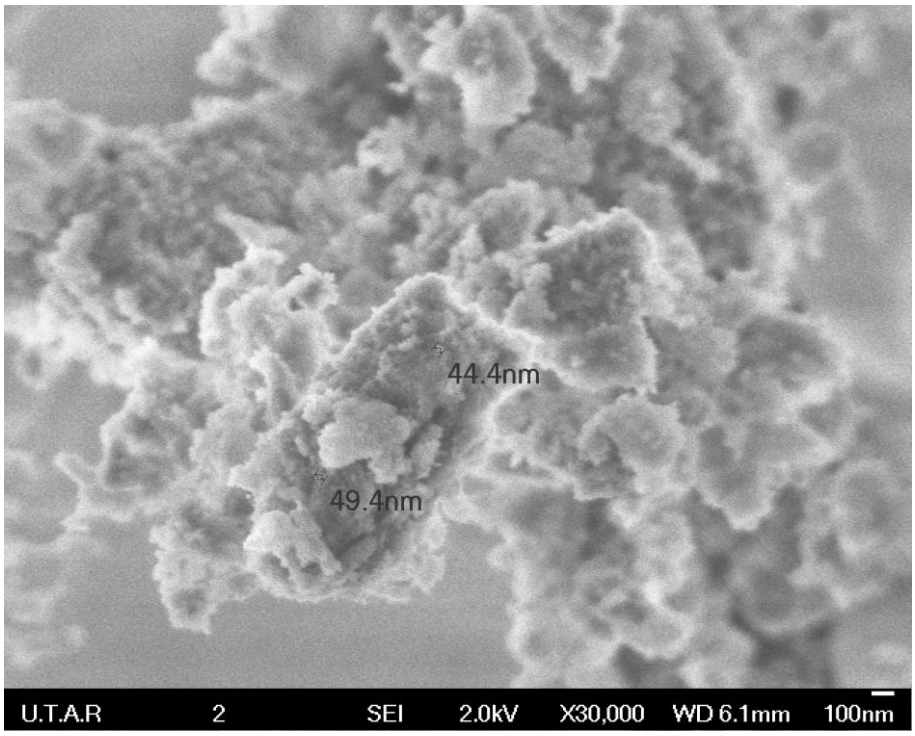

(a)

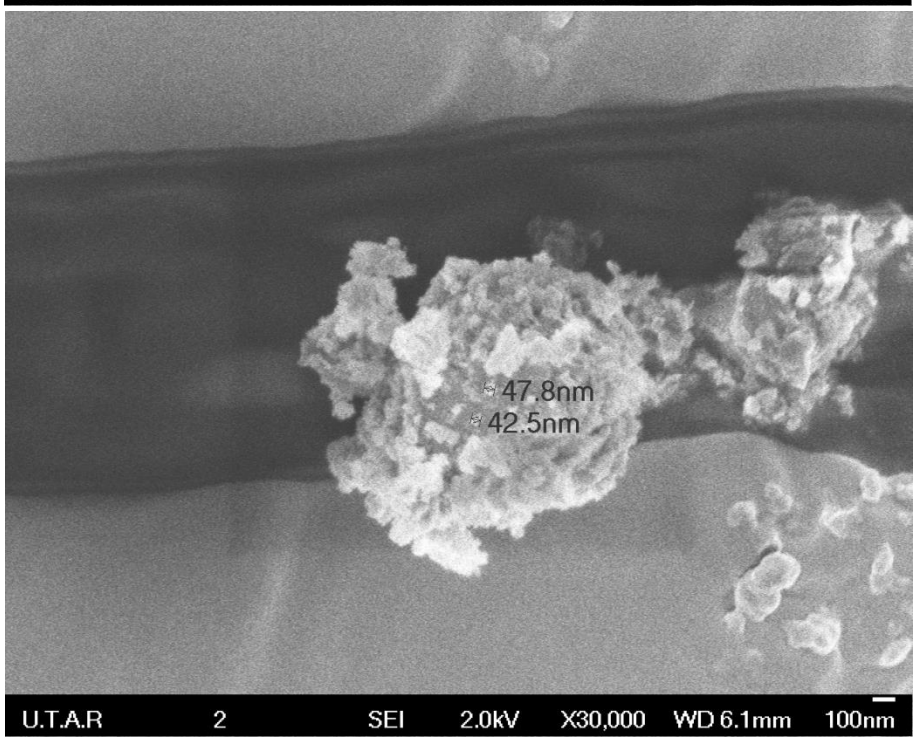

(b)

Figure 4.9: FESEM Images (a) 1Pt:1Pd/Al_2O_3-Coimp (b) 4Pt:1Pd/Al_2O_3-Coimp

Nevertheless, EDXS analysis was still conducted to observe the dispersion of metal nanoparticles on alumina support. High resolution FESEM images and EDXS nanoparticles maps of 1Pt:1Pd/Al_2O_3-Coimp, 4Pt:1Pd/Al_2O_3-Coimp and 1Pt:1Pd/Al_2O_3-Seq are given by Figure 4.10, Figure 4.11 and Figure 4.12 respectively. By referring to all EDXS maps, it can be seen that both platinum and palladium are well dispersed across the alumina surface. Supplementary information about SEM and EDXS are provided in Appendix E.

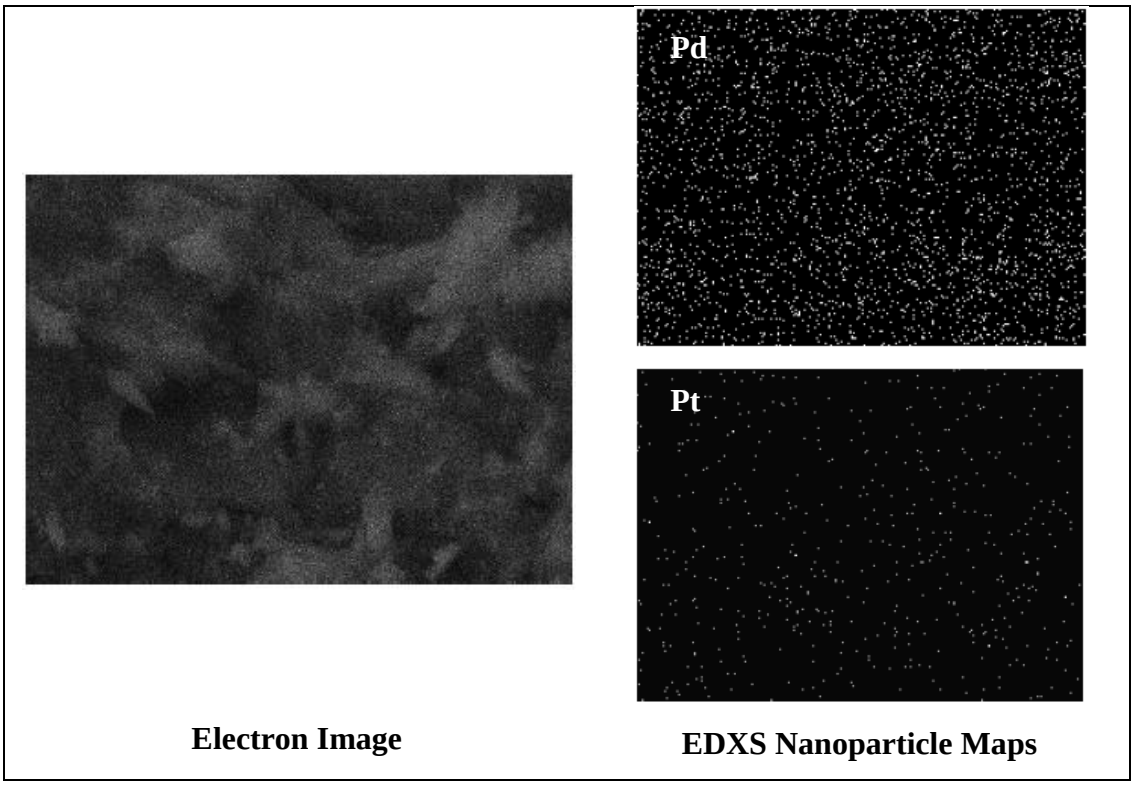

Figure 4.10: FESEM Image and EDXS Nanoparticle Maps of 1Pt:1Pd/Al_2O_3-Coimp

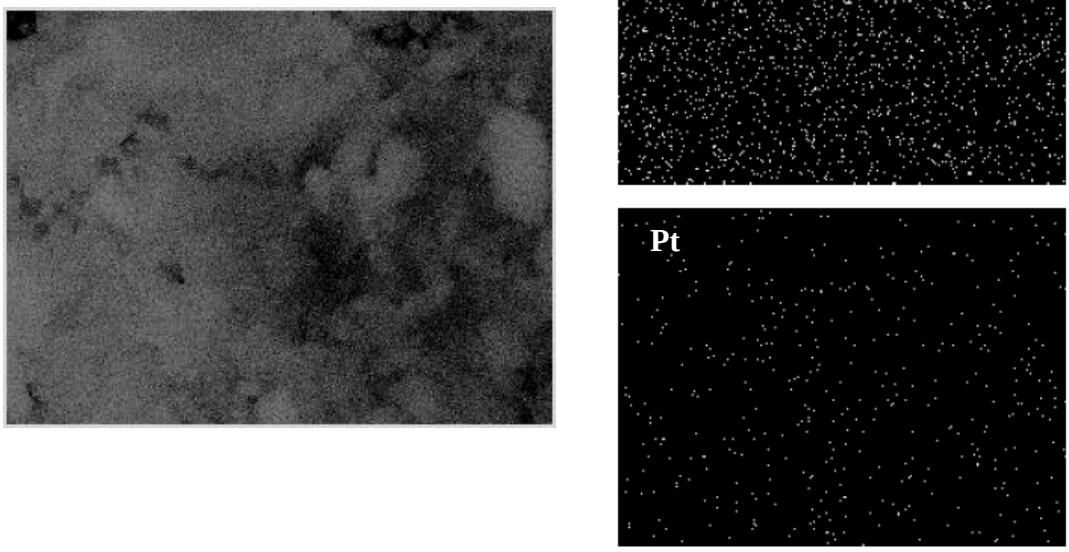

Figure 4.11: FESEM Image and EDXS Nanoparticle Maps of 4Pt:1Pd/Al_2O_3-Coimp

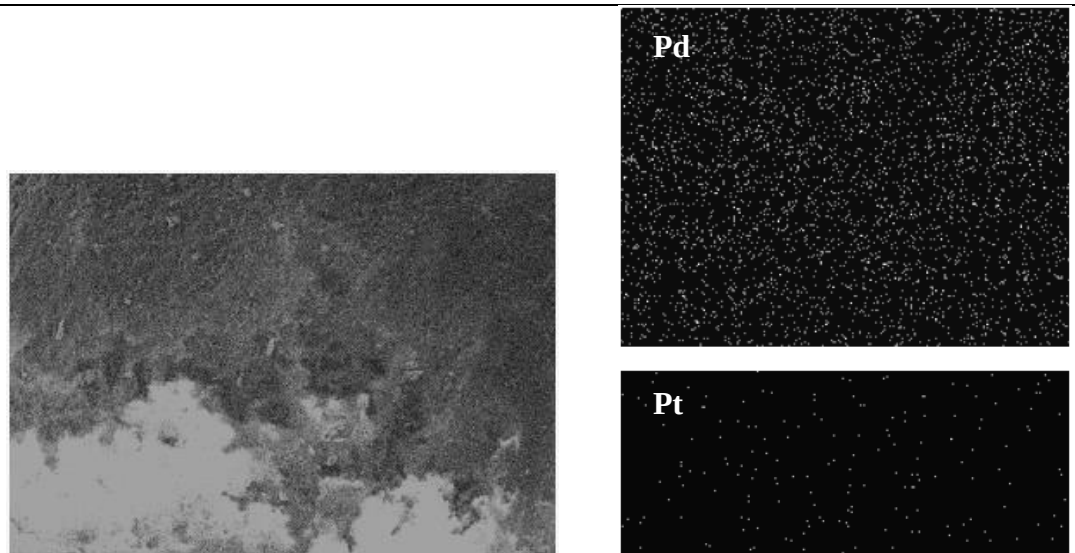

Figure 4.12: FESEM Image and EDXS Nanoparticle Maps of 1Pt:1Pd/Al_2O_3-Seq

CHAPTER 5

CONCLUSION AND RECOMMENDATIONS

5.1 Conclusion

The present project has prepared an array of bimetallic Pd-Pt/Al_2O_3 catalysts using charge-enhanced dry impregnation (CEDI) method. The effect of atomic ratio of Pt:Pd as well as the effect of impregnation method were investigated. Characterisation of the prepared catalysts was conducted using X-ray diffraction (XRD), temperature programmed reduction (TPR), scanning electron microscopy (SEM) and energy-dispersive X-ray spectroscopy (EDXS). On the basis of the results of this project, it was concluded that:

a) Bimetallic Pd-Pt/Al_2O_3 catalysts with high dispersion of nanosized palladium and platinum particles were achieved by CEDI method.
b) Catalysts with higher atomic ratio of Pt:Pd resulted in lower reducibility.
c) Catalysts prepared by sequential impregnation resulted in lower reducibility than the ones prepared by coimpregnation which indicates that core-shell structure could be synthesised using sequential impregnation while alloy structure could be synthesised using coimpregnation.

5.2 Recommendations

Admittedly this project is not perfect. There are still many grey areas left unsolved. Recommendations listed below are suggested for future researchers to uncover more findings on the characteristics of the prepared Pd-Pt/Al_2O_3 catalysts:

a) To better identify the phase of platinum and palladium particles that are absorbed on the alumina support, a transmission electron microscopy (TEM) should be conducted. Materials of different densities can be distinguished based on the darkness of spots. TEM is also useful in determining the particle size distribution of the metal particles. More importantly, with the help of energy-dispersive X-ray spectroscopy (EDXS), TEM can effectively confirm the presence of core-shell structure in sequential impregnated catalysts.
b) An X-ray diffraction (XRD) analysis on the prepared catalysts should be carried out to study the phase of platinum and palladium particles.
c) Moreover, a thermal aging experiment is suggested in order to find out how different atomic ratios of Pt:Pd and different impregnation methods affect sintering of metal nanoparticles.
d) A reactivity test using a fixed bed reactor is suggested in order to assess and compare the catalytic activity of the prepared catalysts.
e) A pulsed chemisorption should be conducted to quantify the dispersion of metal particles on alumina. This enables the investigation of how atomic ratio of Pt:Pd and different impregnation methods affect dispersion of metal particles.

REFERENCES

Abello, M.C., Velasco, A.P., Gorriz, O.F. and Rivarola, J.B., 1995. Temperature-programmed desorption study of the acidic properties of γ-alumina. *Applied Catalysis A: General*, [online] 129(1), pp.93–100. Available at: <http://www.sciencedirect.com/science/article/pii/0926860X95000917> [Accessed 13 Apr. 2015].

Ahlström-Silversand, A.F. and Odenbrand, C.U.I., 1997. Thermally sprayed wire-mesh catalysts for the purification of flue gases from small-scale combustion of bio-fuel Catalyst preparation and activity studies. *Applied Catalysis A: General*, [online] 153(1-2), pp.177–201. Available at: <http://www.sciencedirect.com/science/article/pii/S0926860X96003298> [Accessed 13 Apr. 2015].

Alshaibani, A., Yaakob, Z., Alsobaai, A. and Sahri, M., 2013. Effect of chemically reduced palladium supported catalyst on sunflower oil hydrogenation conversion and selectivity. *Arabian Journal of Chemistry*, pp.2–6.

Amorim, C., Wang, X. and Keane, M. a., 2011. Application of Hydrodechlorination in Environmental Pollution Control: Comparison of the Performance of Supported and Unsupported Pd and Ni Catalysts. *Chinese Journal of Catalysis*, 32(5), pp.746–755.

Augustine, R.L., 1995. *Heterogeneous Catalysis for the Synthetic Chemist*. Chemical Industries. [online] Taylor & Francis. Available at: <http://books.google.com.my/books?id=Nam8OVqKaXIC>.

Auvray, X. and Olsson, L., 2015. Applied Catalysis B : Environmental Stability and activity of Pd- , Pt- and Pd – Pt catalysts supported on alumina for NO oxidation. 169, pp.342–352.

Babu, N.S., Lingaiah, N., Kumar, J.V. and Prasad, P.S.S., 2009. Studies on alumina supported Pd-Fe bimetallic catalysts prepared by deposition-precipitation method for hydrodechlorination of chlorobenzene. *Applied Catalysis A: General*, 367(1-2), pp.70–76.

Bonarowska, M. and Karpiński, Z., 2008. Characterization of supported Pd-Pt catalysts by chemical probes. *Catalysis Today*, [online] 137(2-4), pp.498–503. Available at: <http://www.sciencedirect.com/science/article/pii/S0920586107007468> [Accessed 10 Apr. 2015].

Campanati, M., Fornasari, G. and Vaccari, A., 2003. Fundamentals in the preparation of heterogeneous catalysts. *Catalysis Today*, 77, pp.299–314.

Castellazzi, P., Groppi, G. and Forzatti, P., 2010. Effect of Pt/Pd ratio on catalytic activity and redox behavior of bimetallic Pt-Pd/Al2O3 catalysts for CH4 combustion. *Applied Catalysis B: Environmental*, [online] 95(3-4), pp.303–311. Available at: <http://linkinghub.elsevier.com/retrieve/pii/S0926337310000147> [Accessed 7 Jan. 2015].

Chantaravitoon, P., Chavadej, S. and Schwank, J., 2004. Pt-Sn/Al2O3 catalysts: effect of catalyst preparation and chemisorption methods on H-2 and O-2 uptake. *Chemical Engineering Journal*, [online] 98(1-2), pp.99–104. Available at: <ISI:000220130600008> [Accessed 7 Jan. 2015].

Chen, M. and Schmidt, L.D., 1979. Morphology and composition of Pt-Pd alloy crystallites on SiO2 in reactive atmospheres. *Journal of Catalysis*, [online] 56(2), pp.198–218. Available at: <http://www.sciencedirect.com/science/article/pii/0021951779901076> [Accessed 13 Apr. 2015].

Cho, H.-R. and Regalbuto, J.R., 2015. The rational synthesis of Pt-Pd bimetallic catalysts by electrostatic adsorption. *Catalysis Today*, [online] 246, pp.143–153. Available at: <http://linkinghub.elsevier.com/retrieve/pii/S0920586114006701>.

Ekstrand, A.G., 1966. *Award Ceremony Speech*. [online] Nobel Lecturers, Chemistry 1901-1921. Available at: <http://www.nobelprize.org/nobel_prizes/chemistry/laureates/1918/press.html> [Accessed 11 Apr. 2015].

Ersson, A., Kušar, H., Carroni, R., Griffin, T. and Järås, S., 2003. Catalytic combustion of methane over bimetallic catalysts a comparison between a novel annular reactor and a high-pressure reactor. *Catalysis Today*, 83(1-4), pp.265–277.

Farnetti, E., Di Monte, R. and Kašpar, J., n.d. Homogeneous and Heterogeneous Catalysis. *Inorganic and Bio-iorganic Chemistry*, 2.

Feltes, T. and Timmons, M., n.d. *A Simple Procedure to Determine Surface Charging Parameters in Aqueous Solutions*.

Fogler, H.S., 2006. *Elements of Chemical Reaction Engineering*. Fourth ed. Elements of Chemical Reaction Engineering. [online] Prentice Hall PTR. Available at: <https://books.google.com.my/books?id=QLt0QgAACAAJ>.

Forzatti, P., 2003. Status and perspectives of catalytic combustion for gas turbines. *Catalysis Today*, [online] 83(1-4), pp.3–18. Available at: <http://www.sciencedirect.com/science/article/pii/S0920586103002116> [Accessed 13 Apr. 2015].

Gogate, P.R. and Kabadi, A.M., 2009. A review of applications of cavitation in biochemical engineering/biotechnology. *Biochemical Engineering Journal*,

[online] 44(1), pp.60–72. Available at: <http://www.sciencedirect.com/science/article/pii/S1369703X08003392> [Accessed 13 Apr. 2015].

Haber, J., 1991. Commission on Colloid and Surface Chemistry Manual on Catalyst. *Manual on catalyst characterization (Recommendations 1991)*, [online] 63(9), pp.1227–1246. Available at: <http://pac.iupac.org/publications/pac/pdf/1991/pdf/6309x1227.pdf>.

Haber, J., Block, J.H. and Delmon, B., 1995. Manual of methods and procedures for catalyst characterization (Technical Report). *Pure and Applied Chemistry*, 67(8-9), pp.1257–1306.

Heise, M.. and Schwarz, J.., 1985. Preparation of metal distributions within catalyst supports. I. Effect of ph on catalytic metal profiles. *Journal of Colloid and Interface Science*, [online] 107(1), pp.237–243. Available at: <http://www.sciencedirect.com/science/article/pii/0021979785901675> [Accessed 7 Apr. 2015].

Hermans, L.A.M. and Geus, J.W., 1979. *Preparation of Catalysts II, Proceedings of the Second International Symposium*. Studies in Surface Science and Catalysis. [online] *Studies in Surface Science and Catalysis*, Elsevier. Available at: <http://www.sciencedirect.com/science/article/pii/S0167299109602081> [Accessed 12 Apr. 2015].

Hohl, H. and Stumm, W., 1976. Interaction of Pb2+ with hydrous γ-Al2O3. *Journal of Colloid and Interface Science*, [online] 55(2), pp.281–288. Available at: <http://www.sciencedirect.com/science/article/pii/0021979776900357> [Accessed 13 Apr. 2015].

Hussain, S.T., Mazhar, M., Hasib-ur-Rahman, M. and Bari, M., 2009. Trimetallic supported catalyst for renewable source of energy and environmental control through CO2 conversion. *Environmental Technology*, [online] 30(6), pp.543–559. Available at: <http://dx.doi.org/10.1080/09593330902806624>.

Hwang, C.P. and Yeh, C.T., 1996. Platinum-oxide species formed by oxidation of platinum crystallites supported on alumina. *Journal of Molecular Catalysis A: Chemical*, 112(2), pp.295–302.

Jiang, H., Yang, H., Hawkins, R. and Ring, Z., 2007. Effect of palladium on sulfur resistance in Pt-Pd bimetallic catalysts. *Catalysis Today*, 125, pp.282–290.

De Jong, K.P., 2009. *Synthesis of Solid Catalysts*. Weinheim: Wiley-VCH.

De Jong, K.P. and Geus, J.W., 1982. Production of supported silver catalysts by liquid-phase reduction. *Applied Catalysis*, [online] 4(1), pp.41–51. Available at: <http://www.sciencedirect.com/science/article/pii/0166983482802881> [Accessed 12 Apr. 2015].

Jun, K.-W., Lee, Y.-J., Kim, S.-M. and Kim, J.Y., 2009. *Method of Preparing Boehmite and Gamma-Alumina with High Surface Area*. US 2009/0104108 A1.

Komiyama, M., Merrill, R.P. and Hansberger, H.F., 1980. Concentration profiles in impregnation of porous catalysts: Nickel on alumina. *Journal of Catalysis*, [online] 63(1), pp.35–52. Available at: <http://www.sciencedirect.com/science/article/pii/0021951780900585> [Accessed 13 Apr. 2015].

Koptyug, I.., Kabanikhin, S.., Iskakov, K.., Fenelonov, V.., Khitrina, L.Y., Sagdeev, R.. and Parmon, V.., 2000. A quantitative NMR imaging study of mass transport in porous solids during drying. *Chemical Engineering Science*, [online] 55(9), pp.1559–1571. Available at: <http://www.sciencedirect.com/science/article/pii/S0009250999004042> [Accessed 4 Mar. 2015].

Leofanti, G., Tozzola, G., Padovan, M., Petrini, G., Bordiga, S. and Zecchina, A., 1997. Catalyst characterization: applications. *Catalysis Today*, [online] 34(3-4), pp.329–352. Available at: <http://www.sciencedirect.com/science/article/pii/S0920586197860890> [Accessed 13 Apr. 2015].

Li, C. and Chen, Y.-W., 1995. Temperature-programmed-reduction studies of nickel oxide/alumina catalysts: effects of the preparation method. *Thermochimica Acta*, 256, pp.457–465.

Li, G., Hu, L. and Hill, J.M., 2006. Comparison of reducibility and stability of alumina-supported Ni catalysts prepared by impregnation and co-precipitation. *Applied Catalysis A: General*, 301(1), pp.16–24.

Li, T., Zhang, W., Lee, R.Z. and Zhong, Q., 2009. Nickel-boron alloy catalysts reduce the formation of Trans fatty acids in hydrogenated soybean oil. *Food Chemistry*, [online] 114(2), pp.447–452. Available at: <http://linkinghub.elsevier.com/retrieve/pii/S0308814608011588> [Accessed 7 Jan. 2015].

Lieske, H., Lietz, G., Spindler, H. and Volter, J., 1983. Reactions of platinum in oxygen- and hydrogen-treated Pt/gamma-Al2O3 catalysts I. Temperature-programmed reduction, adsorption, and redispersion of platinum. *Journal of Catalysis*, [online] 81(1), pp.8–16. Available at: <http://www.sciencedirect.com/science/article/pii/0021951783901422> [Accessed 10 Apr. 2015].

Lieske, H. and Volter, J., 1985. Pd Redispersion by Spreading of PdO in O2 Treated Pd/Al2O3. *Journal of Physical Chemistry*, 89(10), pp.1983–1984.

Lingaiah, N., Sai Prasad, P.., Kanta Rao, P., Berry, F.. and Smart, L.., 2002. Structure and activity of microwave irradiated silica supported Pd–Fe bimetallic catalysts in the hydrodechlorination of chlorobenzene. *Catalysis Communications*, [online] 3(9), pp.391–397. Available at:

<http://www.sciencedirect.com/science/article/pii/S1566736702001590> [Accessed 10 Apr. 2015].

Loiha, S., Klysubun, W., Khemthong, P., Prayoonpokarach, S. and Wittayakun, J., 2011. Reducibility of Ni and NiPt supported on zeolite beta investigated by XANES. *Journal of the Taiwan Institute of Chemical Engineers*, 42(3), pp.527–532.

Long, N.V., Hien, T.D., Asaka, T., Ohtaki, M. and Nogami, M., 2011. Synthesis and characterization of Pt-Pd nanoparticles with core-shell morphology: Nucleation and overgrowth of the Pd shells on the as-prepared and defined Pt seeds. *Journal of Alloys and Compounds*, [online] 509(29), pp.7702–7709. Available at: <http://dx.doi.org/10.1016/j.jallcom.2011.04.031>.

Mang, T., Breitscheidel, B., Polanek, P. and Knözinger, H., 1993. Adsorption of platinum complexes on silica and alumina: Preparation of non-uniform metal distributions within support pellets. *Applied Catalysis A: General*, [online] 106(2), pp.239–258. Available at: <http://www.sciencedirect.com/science/article/pii/0926860X9380180X> [Accessed 7 Apr. 2015].

Morbidelli, M., Gavriilidis, A. and Varma, A., 2005. *Catalyst Design: Optimal Distribution of Catalyst in Pellets, Reactors, and Membranes*. Cambridge Series in Chemical Engineering. [online] Cambridge University Press. Available at: <http://books.google.com.my/books?id=z79X0CEYw1gC>.

Narui, K., Yata, H., Furuta, K., Nishida, A., Kohtoku, Y. and Matsuzaki, T., 1999. Effects of addition of Pt to PdO/Al2O3 catalyst on catalytic activity for methane combustion and TEM observations of supported particles. *Applied Catalysis A: General*, 179(1-2), pp.165–173.

Neimark, A. V, Kheifets, L.I. and Fenelonov, V.B., 1981. Theory of preparation of supported catalysts. *Industrial & Engineering Chemistry Product Research and Development*, [online] 20(3), pp.439–450. Available at: <http://dx.doi.org/10.1021/i300003a006>.

Park, J. and Regalbuto, J.R., 1995. A simple, accurate determination of oxide PZC and the strong buffering effect of oxide surfaces at incipient wetness. *Journal of colloid and interface science*, [online] 175, pp.239–252. Available at: <http://www.scopus.com/inward/record.url?eid=2-s2.0-0000691707&partnerID=40&md5=485d01473de654db29f0316728ece31b\nhttp://www.sciencedirect.com/science/article/pii/S002197978571452X>.

Perego, C. and Villa, P., 1997. Catalyst preparation methods. 34, pp.281–305.

Perkas, N., Gunawan, P., Amirian, G., Wang, Z., Zhong, Z. and Gedanken, A., 2014. The sonochemical approach improves the CuO-ZnO/TiO(2) catalyst for WGS reaction. *Physical chemistry chemical physics : PCCP*, [online] 16(16), pp.7521–30. Available at: <http://www.ncbi.nlm.nih.gov/pubmed/24626876> [Accessed 7 Jan. 2015].

Persson, K., 2006. *Bimetallic Palladium Catalysts for Methane Combustion in Gas Turbines*.

Persson, K., Jansson, K. and Järås, S.G., 2007. Characterisation and microstructure of Pd and bimetallic Pd-Pt catalysts during methane oxidation. *Journal of Catalysis*, [online] 245(2), pp.401–414. Available at: <http://linkinghub.elsevier.com/retrieve/pii/S0021951706003848> [Accessed 7 Jan. 2015].

Qin, Q. and Ramkrishna, D., 2005. The Effect of Operating Conditions on the Dispersion State of Supported Metal Catalysts: A Model Study†. *Industrial & Engineering Chemistry Research*, [online] 44(16), pp.6466–6476. Available at: <http://dx.doi.org/10.1021/ie048954b>.

Radziuk, D., Möhwald, H. and Shchukin, D., 2008. Ultrasonic Activation of Platinum Catalysts. *The Journal of Physical Chemistry C*, [online] 112(49), pp.19257–19262. Available at: <http://dx.doi.org/10.1021/jp806508t>.

Regalbuto, J., 2007. *CATALYST Science and Engineering*. [online] *Catalyst Preparation Science and Engineering*. Boca Raton: CRC Press. Available at: <http://scholar.google.com/scholar?hl=en&btnG=Search&q=intitle:Catalyst+Preparation+Science+and+Engineering#0>.

Reyes, P., Figueroa, A., Pecchi, G. and Fierro, J.L.., 2000. Catalytic combustion of methane on Pd–Cu/SiO2 catalysts. *Catalysis Today*, [online] 62(2-3), pp.209–217. Available at: <http://www.sciencedirect.com/science/article/pii/S0920586100004223> [Accessed 13 Apr. 2015].

Ross, J.R.H., 2012. *Heterogeneous Catalysis - Fundamentals and Applications*. *Elsevier*. Oxford: Elsevier.

Roth, D., Gélin, P., Primet, M. and Tena, E., 2000. Catalytic behaviour of Cl-free and Cl-containing Pd/Al2O3 catalysts in the total oxidation of methane at low temperature. *Applied Catalysis A: General*, [online] 203(1), pp.37–45. Available at: <http://www.sciencedirect.com/science/article/pii/S0926860X00004658> [Accessed 13 Apr. 2015].

Rozita, Y., Brydson, R. and Scott, a J., 2010. Nanoparticles. *Journal of Physics: Conference Series*, 241(Emag 2009), p.012096.

Ruan, Q., Zhu, Y., Zeng, Y., Qian, H., Xiao, J., Xu, F., Zhang, L. and Zhao, D., 2009. Ultrasonic-irradiation-assisted oriented assembly of ordered monetite nanosheets stacking. *The journal of physical chemistry. B*, 113(4), pp.1100–1106.

Shafii, S., Lihua, W., Nordin, M.R. and Yong, L.K., 2012. Synthesis of Palladium-Platinum Bimetallic Nanoparticles and their Catalytic Activity towards the Hydrogenation Reaction of Palm Olein. *Journal of Chemical Engineering & Process Technology*, [online] 03(01), pp.1–8. Available at:

<http://www.omicsonline.org/2157-7048/2157-7048-3-123.digital/2157-7048-3-123.html> [Accessed 7 Jan. 2015].

Shah, A.M. and Regalbuto, J.R., 1994. Retardation of Pt Adsorption over Oxide Supports at pH Extremes: Oxide Dissolution or High Ionic Strength? *Langmuir : the ACS journal of surfaces and colloids*, 10(2), pp.500–504.

Singh, D., Rezac, M.E. and Pfromm, P.H., 2010. Partial hydrogenation of soybean oil using metal-decorated integral-asymmetric polymer membranes: Effects of morphology and membrane properties. *Journal of Membrane Science*, [online] 348(1-2), pp.99–108. Available at: <http://www.sciencedirect.com/science/article/pii/S0376738809007881> [Accessed 12 Apr. 2015].

Spieker, W. a. and Regalbuto, J.R., 2001. A fundamental model of platinum impregnation onto alumina. *Chemical Engineering Science*, 56, pp.3491–3504.

Stanković, M., Gabrovska, M., Krstić, J., Tzvetkov, P., Shopska, M., Tsacheva, T., Banković, P., Edreva-Kardjieva, R. and Jovanović, D., 2009. Effect of silver modification on structure and catalytic performance of Ni-Mg/diatomite catalysts for edible oil hydrogenation. *Journal of Molecular Catalysis A: Chemical*, [online] 297(1), pp.54–62. Available at: <http://www.sciencedirect.com/science/article/pii/S1381116908003920> [Accessed 12 Apr. 2015].

Strobel, R., Grunwaldt, J.D., Camenzind, A., Pratsinis, S.E. and Baiker, A., 2005. Flame-made alumina supported Pd-Pt nanoparticles: Structural properties and catalytic behavior in methane combustion. *Catalysis Letters*, 104(1-2), pp.9–16.

Suslick, K.S., 2000. Sonochemistry: A physical perspective. In: *NONLINEAR ACOUSTICS AT THE TURN OF THE MILLENNIUM: ISNA 15, 15th International Symposium*. AIP Publishing, pp.95–104.

Tao, F., Grass, M.E., Zhang, Y., Butcher, D.R., Renzas, J.R., Liu, Z., Chung, J.Y., Mun, B.S., Salmeron, M. and Somorjai, G.A., 2008. Reaction-Driven Restructuring of Rh-Pd and Pt-Pd Core-Shell Nanoparticles. *Science*, 322, pp.932–934.

Toukoniitty, B., Kuusisto, J., Mikkola, J.-P., Salmi, T. and Murzin, D.Y., 2005. Effect of Ultrasound on Catalytic Hydrogenation of d-Fructose to d-Mannitol. *Industrial & Engineering Chemistry Research*, [online] 44(25), pp.9370–9375. Available at: <http://dx.doi.org/10.1021/ie050190s>.

Vinodgopal, K., Neppolian, B., Lightcap, I. V, Grieser, F., Ashokkumar, M. and Kamat, P. V, 2010. Sonolytic Design of Graphene−Au Nanocomposites. Simultaneous and Sequential Reduction of Graphene Oxide and Au(III). *The Journal of Physical Chemistry Letters*, [online] 1(13), pp.1987–1993. Available at: <http://dx.doi.org/10.1021/jz1006093>.

Wang, L. and Hall, W.K., 1982. The preparation and genesis of molybdena-alumina and related catalyst systems. *Journal of Catalysis*, [online] 77(1), pp.232–241. Available at: <http://www.sciencedirect.com/science/article/pii/0021951782901634> [Accessed 13 Apr. 2015].

Yamamoto, H. and Uchida, H., 1998. Oxidation of methane over Pt and Pd supported on alumina in lean-burn natural-gas engine exhaust. *Catalysis Today*, [online] 45(1-4), pp.147–151. Available at: <http://www.sciencedirect.com/science/article/pii/S092058619800265X> [Accessed 13 Apr. 2015].

Yu, W., Porosoff, M.D. and Chen, J.G., 2012. Review of Pt-based bimetallic catalysis: From model surfaces to supported catalysts. *Chemical Reviews*, 112(11), pp.5780–5817.

Zhu, X., Cho, H., Pasupong, M. and Regalbuto, J.R., 2013. Charge-Enhanced Dry Impregnation: A Simple Way to Improve the Preparation of Supported Metal Catalysts. pp.1–6.

APPENDICES

APPENDIX A: Calculation on Surface Loading

Surface loading, *SL* (m^2/L) is defined as:

$$SL\ (m^2/L) = \frac{m(g) \times A(m^2/g)}{V(L)} \quad \text{(A.1)}$$

where

m = mass of oxide support, g

A = specific surface area of support, m^2/g

V = volume of impregnating solution, L

Sample calculation

Assume

A = 200 m^2/g

m = 0.05 g

V = 200 mL

Calculation

$$SL = \frac{m \times A}{V}$$

$$= \frac{0.05 \times 200}{0.2}$$

$$= \mathbf{50\ m^2/L}$$

In dry impregnation, the volume of impregnating solution equals to the pore volume of the support. Hence, the surface loading is reduced to:

$$SL(m^2/L) = \frac{A(m^2/g)}{PV(L/g)} \quad \text{(A.2)}$$

where

A = specific surface area of support, m^2/g

PV = volume of impregnating solution, L/g

Calculation on the *SL* employed in the preparation of Pd-Pt/Al_2O_3

Assume

A = 200 m^2/g

PV = 0.45 mL/g

Calculation

$$SL = \frac{A}{PV}$$

$$= \frac{200}{0.00045}$$

$$=\mathbf{444444\ m^2/L}$$

APPENDIX B: Supplementary Data for the Determination of Point of Zero Charge

Data for the determination of point of zero charge (PZC) of γ-alumina is tabulated in Table B.1.

Table B.1: pH Shifts

Initial pH	**Final pH**		
	***SL* = 50 m^2/L**	***SL* = 500 m^2/L**	***SL* = 1000 m^2/L**
1.93	2.14	2.08	2.35
2.51	2.70	2.71	3.15
3.56	3.80	6.32	7.34
4.74	7.40	6.90	7.66
5.71	7.16	7.31	7.82
6.59	7.12	8.42	7.72
7.20	7.53	8.64	8.07
8.92	8.47	8.80	8.65
9.46	9.10	8.72	7.72
10.43	10.33	9.84	8.88
11.10	10.90	10.47	9.84

APPENDIX C: Supplementary Data for the Determination of pH for Optimal Adsorption

Data for the determination of pH for optimal adsorption of platinum and palladium is tabulated in Table C.1 and Table C.2 respectively. Take note that the surface loading applied was 600 m^2/L.

Table C.2: Adsorption Density of Platinum

pH		**Concentration (µg/L)**		**Adsorption Density, *Γ***
Final	**Initial**	**Final**	**Initial**	**(nmol/m^2)**
1.62	1.62	82.53	98.68	0.1380
3.13	9.03	165.10	227.30	0.5314
3.63	3.58	61.70	78.61	0.1445
3.66	3.96	71.86	106.90	0.2994
4.23	4.99	46.78	65.60	0.1608
5.62	4.86	148.30	149.80	0.0128
6.35	7.46	124.80	149.60	0.2119
6.81	7.66	110.30	141.40	0.2657
8.05	9.75	141.30	151.80	0.0897
10.88	10.66	281.30	285.60	0.0367

Table C.2: Adsorption Density of Palladium

pH		Concentration (µg/L)		Adsorption Density, Γ
Final	**Initial**	**Final**	**Initial**	**(nmol/m^2)**
0.89	0.96	142.30	162.60	0.3179
1.88	1.45	77.90	154.00	1.1918
2.08	1.81	108.50	177.60	1.0822
2.82	2.90	63.19	145.60	1.2906
3.10	2.96	83.04	176.50	1.4637
3.58	3.33	72.57	139.70	1.0513
3.81	5.52	51.95	80.56	0.4481
4.53	4.77	19.00	55.95	0.5787
5.61	4.39	45.49	90.89	0.7110
6.13	5.69	42.90	44.50	0.0251

Sample calculation on adsorption density

Adsorption density, Γ (nmol/m^2) is defined as:

$$\Gamma(\text{nmol/m}^2) = \frac{(C_{initial} - C_{final})(\text{µg/L}) \times 10^3(\text{nmol/µmol})}{\text{SL}\ (\text{m}^2/\text{L}) \times MW\ (\text{µg/µmol})} \qquad \text{(C.1)}$$

where

$C_{initial}$ = initial concentration of impregnating solution, µg/L

C_{final} = final concentration of impregnating solution, µg/L

MW = molecular weight of metal, µg/µmol

SL = surface loading of oxide support, m^2/L

Take the adsorption density data of platinum at final pH of 1.62 in Table C.1 as an example,

$C_{initial}$ = 98.68 μg/L

C_{final} = 82.53 μg/L

MW = 195.08 μg/μmol

SL = 600 m^2/L

$$\Gamma(\mathrm{nmol/m^2}) = \frac{(C_{initial} - C_{final})(\mu g/L) \times 10^3(nmol/\mu mol)}{SL\ (m^2/L) \times MW\ (\mu g/\mu mol)}$$

$$= \frac{(98.68 - 82.53)(\mu g/L) \times 10^3(nmol/\mu mol)}{600\ (m^2/L) \times 195.08\ (\mu g/\mu mol)}$$

$$= \mathbf{0.1380\ nmol/m^2}$$

Take the adsorption density data of palladium at final pH of 0.89 in Table C.2 as an example,

$C_{initial}$ = 162.60 μg/L

C_{final} = 142.30 μg/L

MW = 106.42 μg/μmol

SL = 600 m^2/L

$$\Gamma(\mathrm{nmol/m^2}) = \frac{(C_{initial} - C_{final})(\mu g/L) \times 10^3(nmol/\mu mol)}{SL\ (m^2/L) \times MW\ (\mu g/\mu mol)}$$

$$= \frac{(162.60 - 142.30)(\mu g/L) \times 10^3(nmol/\mu mol)}{600\ (m^2/L) \times 106.42\ (\mu g/\mu mol)}$$

$$= \mathbf{0.3179\ nmol/m^2}$$

APPENDIX D: Supplementary Data for the Preparation of Pd-Pt/Al_2O_3 Bimetallic Catalyst

The amount of metal precursors needed to prepare for various Pd-Pt/Al_2O_3 bimetallic catalyst samples is tabulated in Table D.1.

Table D.3: Preparation of Various Pd-Pt/Al_2O_3 Bimetallic Catalyst Samples

Catalyst Name	Nominal Atomic Ratio		Concentration before Mix (g/mL)[a]		Concentration after Mix (g/mL)[a,b]		Mass after Mix[b] (g)		Metal Loading (wt%)	
	Pt	Pd	Pt	Pd	Pt	Pd	Pt	Pd	Pt	Pd
0Pt:1Pd/Al_2O_3	0	1	0.00000	0.00968	0.00000	0.00968	0.00000	0.00436	0.00	0.43
1Pt:0Pd/Al_2O_3	1	0	0.03526	0.00000	0.03526	0.00000	0.01587	0.00000	1.56	0.00
4Pt:1Pd/Al_2O_3-Coimp	4	1	0.09680	0.01307	0.04840	0.00654	0.02178	0.00294	2.13	0.29
1Pt:1Pd/Al_2O_3-Coimp	1	1	0.03526	0.01307	0.01763	0.00654	0.00793	0.00294	0.79	0.29
1Pt:1Pd/Al_2O_3-Seq	1	1	0.01763	0.00654	0.01763	0.00654	0.00793	0.00294	0.79	0.29

[a]Determined by ICP-OES

[b]The word “After Mix” only applies for 4Pt:1Pd/Al_2O_3-Coimp and 1Pt:1Pd/Al_2O_3-Coimp.

Sample Calculation

Take the sample of 4Pt:1Pd/Al_2O_3-Coimp as an example,

Given,

Mass of γ-alumina pellet, m = 1 g

Pore volume of pellet, PV = 0.45 mL/g

Volume of impregnating solution, V = $PV \times m$

= 0.45 mL/g × 1 g

= 0.45 mL

Atomic mass of Pd, M_{Pd} = 106.42 g/mol

Atomic mass of Pt, M_{Pt} = 195.08 g/mol

Concentration of Pt before mix = 0.09680 g/mL

Concentration of Pd before mix = 0.01307 g/mL

Equal volume of Pt and Pd is mixed.

Concentration of Pt after mix = 0.09680 g/mL ÷ 2

= 0.04840 g/mL

Concentration of Pd after mix = 0.01307 g/mL ÷ 2

= 0.00654 g/mL

Mass of Pt after mix, m_{Pt} = Concentration of Pt after mix × V

= 0.04840 g/mL × 0.45 mL

= 0.02178 g

Mass of Pd after mix, m_{Pd} = Concentration of Pd after mix × V

= 0.00654 g/mL × 0.45 mL

= 0.00294 g

Metal loading of Pt = $\frac{m_{Pt}}{m+m_{Pt}} \times 100\%$

= $\frac{0.02178}{1+0.02178} \times 100\%$

= 2.13 wt%

Metal loading of Pd $= \frac{m_{Pd}}{m+m_{Pd}} \times 100\%$

$= \frac{0.00294}{1+0.00294} \times 100\%$

= 0.29 wt%

Atomic ratio of Pt:Pd $= \frac{m_{Pt}/M_{Pt}}{m_{Pd}/M_{Pd}}$

$= \frac{0.02178/195.08}{0.00294/106.42}$

= 4.04:1

Nominal atomic ratio of Pt:Pd = 4:1

APPENDIX E: Raw Data of Characterisation Tests